Electronic Supplementary Material (ESI) for Molecular BioSystems


# Supplementary material: Model-driven experimental analysis of the function of SHP-2 in IL-6-induced Jak/STAT signaling

Anna Dittrich, Tom Quaiser, Christina Khouri, Dieter Görtz, Martin Mönnigmann, Fred Schaper

# Supplementary Information 1: Graphical and mathematical representation of model $M_0$ to $M_7$ and model variants.

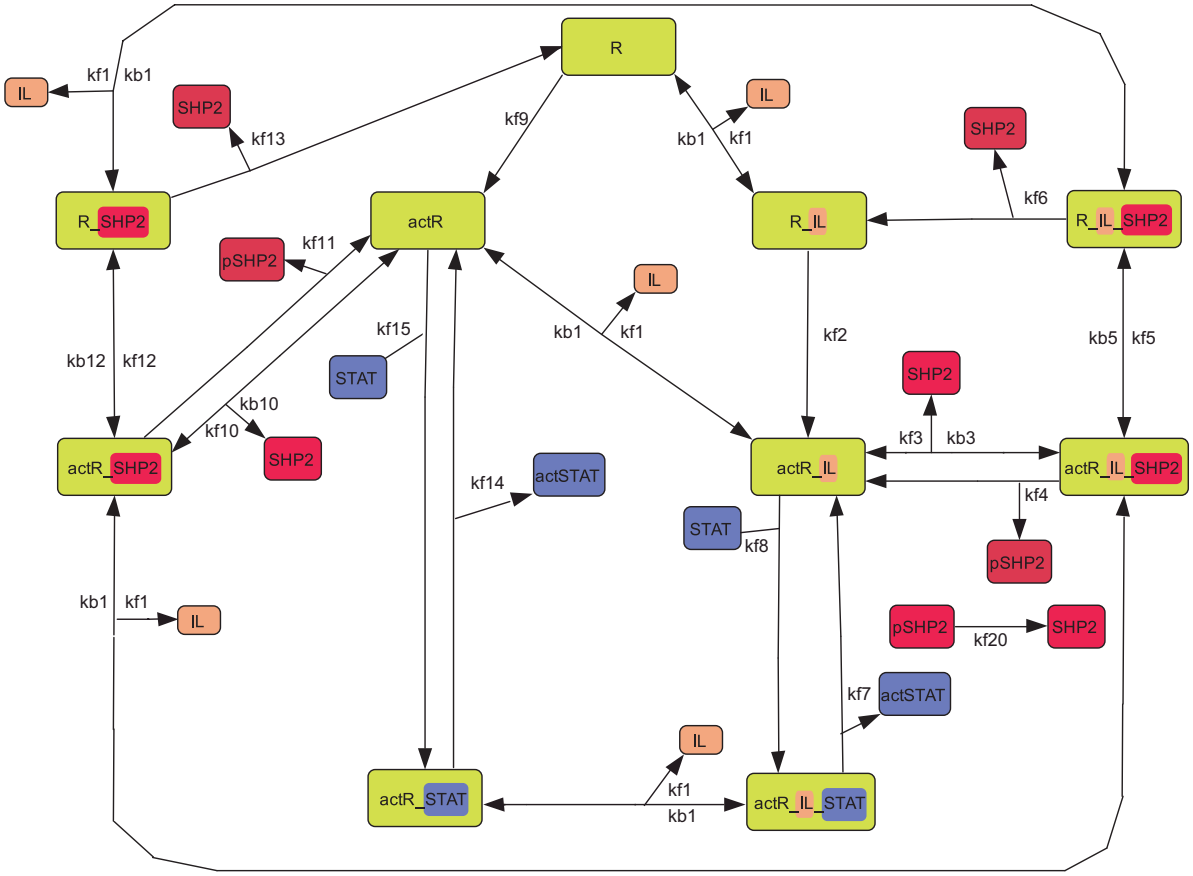


Figure S1: Graphical representation of the initial model. Protein species are depicted as colored rectangles. Arrows between the protein species describe association or dissociation reactions, which follow mass action kinetics. The names of kinetic constants are shown next to the corresponding reaction arrows. A mathematical representation of this model is given in Table S1.

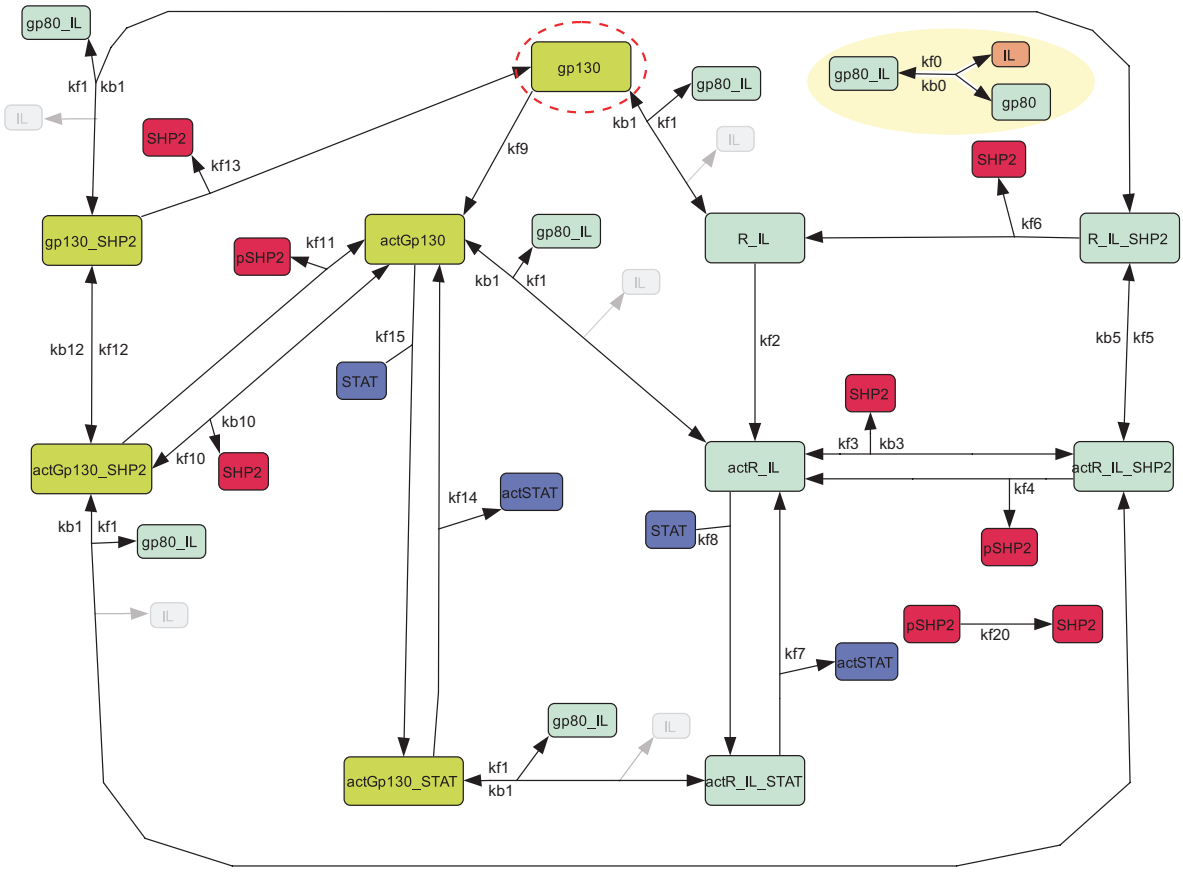


Figure S2: Graphical representation of model $M_1$. The same notation as in Fig. S1 is used. In contrast to $M_0$ the binding of IL-6 to the receptor has been changed. Model $M_1$ is extended for the two receptor subunits gp80 and gp130 (see red dotted circle), which have previously been integrated in one species (R). To activate the pathway in the new model, first a gp80-IL-6 complex needs to be formed (highlighted in yellow), which subsequently binds to gp130. Removed parts from the previous model are shown in gray. A mathematical representation of this model is given in Table S2.

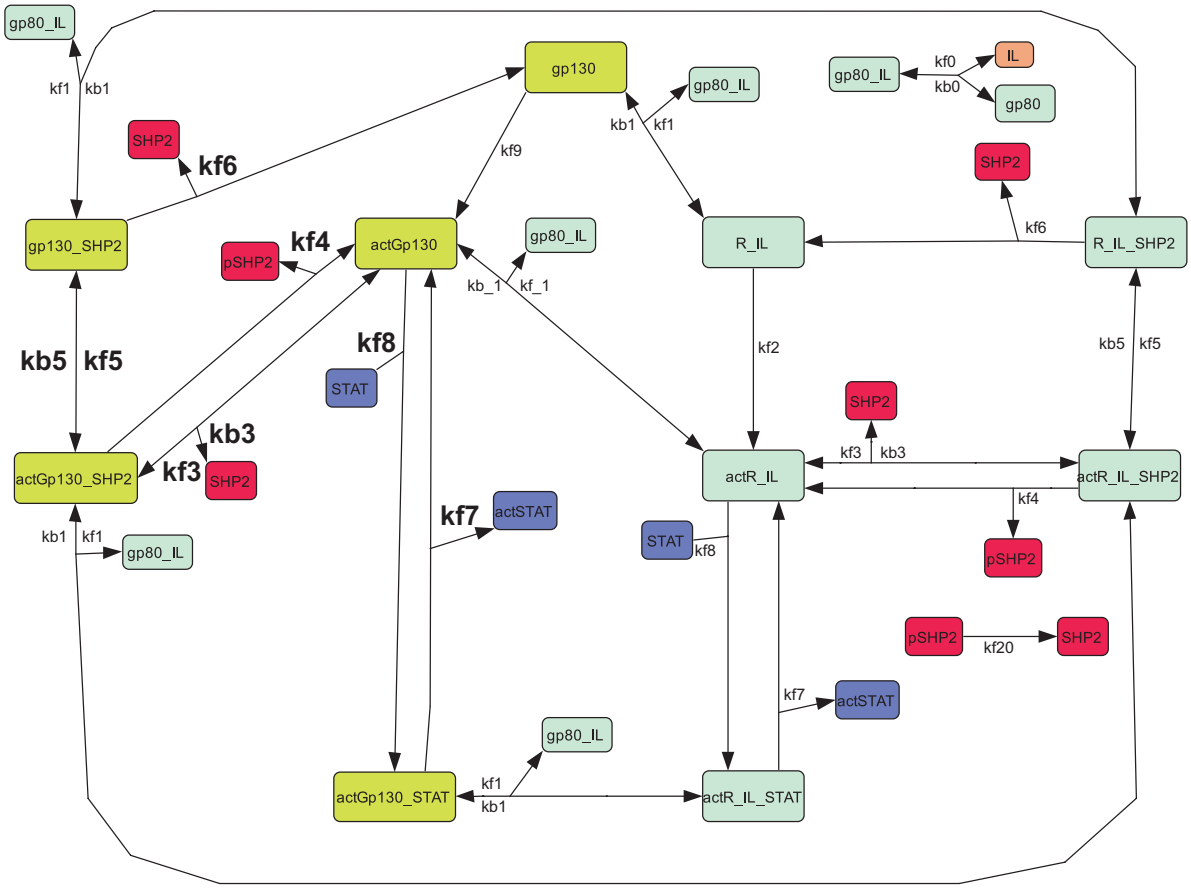


Figure S3: Graphical representation of model $M_2$. The same notation as in the previous figures is used. Model $M_2$ differs from the previous model $M_1$ in assuming identical kinetic constants for STAT (or SHP2) reactions with the receptor, regardless of whether the receptor is in complex with IL-6 or not. The changed parameter names are depicted in bold letters. A mathematical representation of this model is given in Table S3.

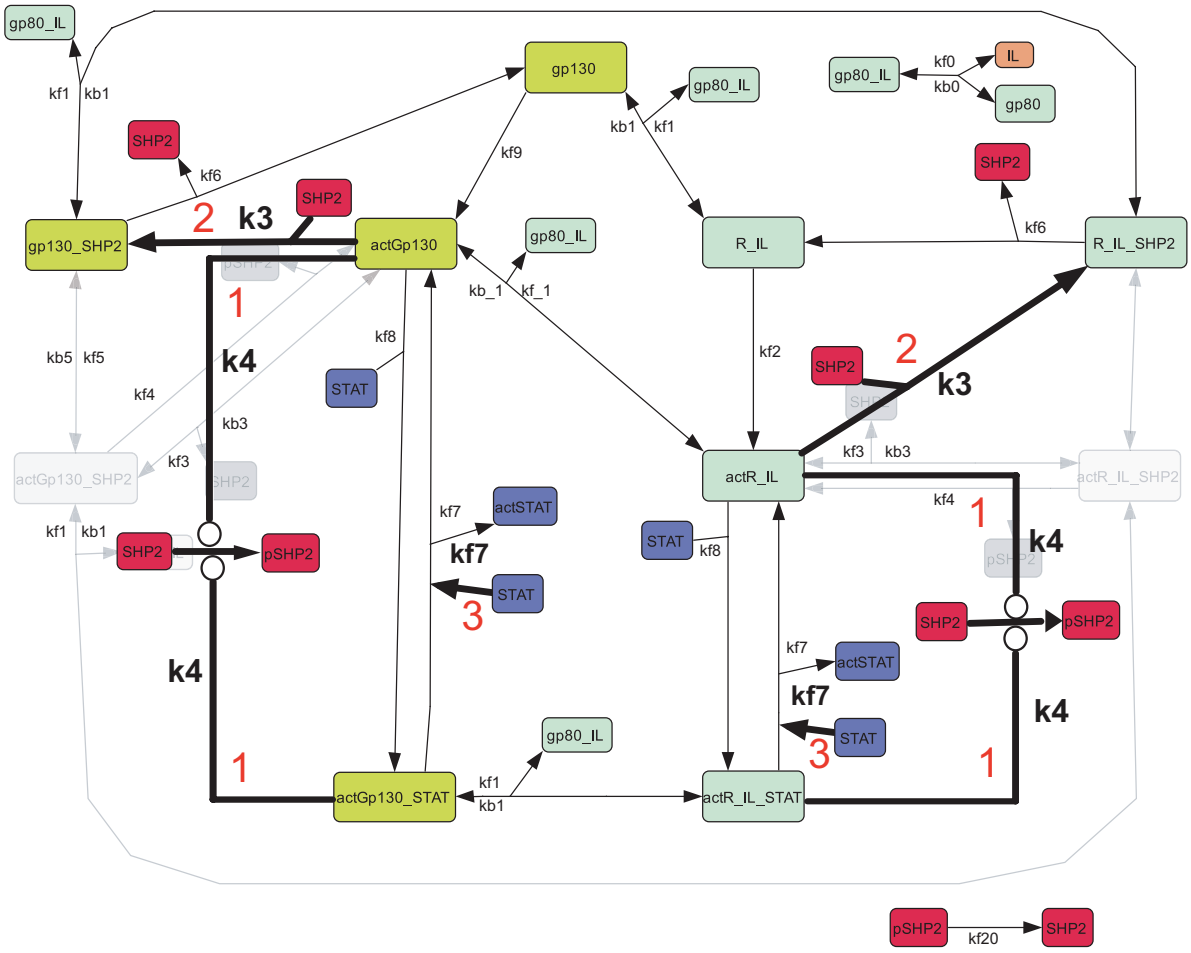


Figure S4: Graphical representation of model $M_3$. The same notation as in the previous figures is used. Two changes to model $M_2$ result in $M_3$. First, the complex formation between SHP2 and active receptor species (actGp130 or actR_IL) has been simplified. The activated receptors now phosphorylate SHP2 in a pseudo first order reaction (see reactions marked with a red 1), in which no complex needs to be formed (see gray model parts). Note that pseudo first order reaction arrows end in circles. This simplification necessitates changes for the SHP2-induced receptor inactivation (see reaction arrows marked with a red 2). Second, STAT is modeled as monomer and only binding of a second STAT to the receptor induces the dissociation of the active dimer actSTAT (see reaction marked with a red 3). A mathematical representation of this model is given in Table S4.

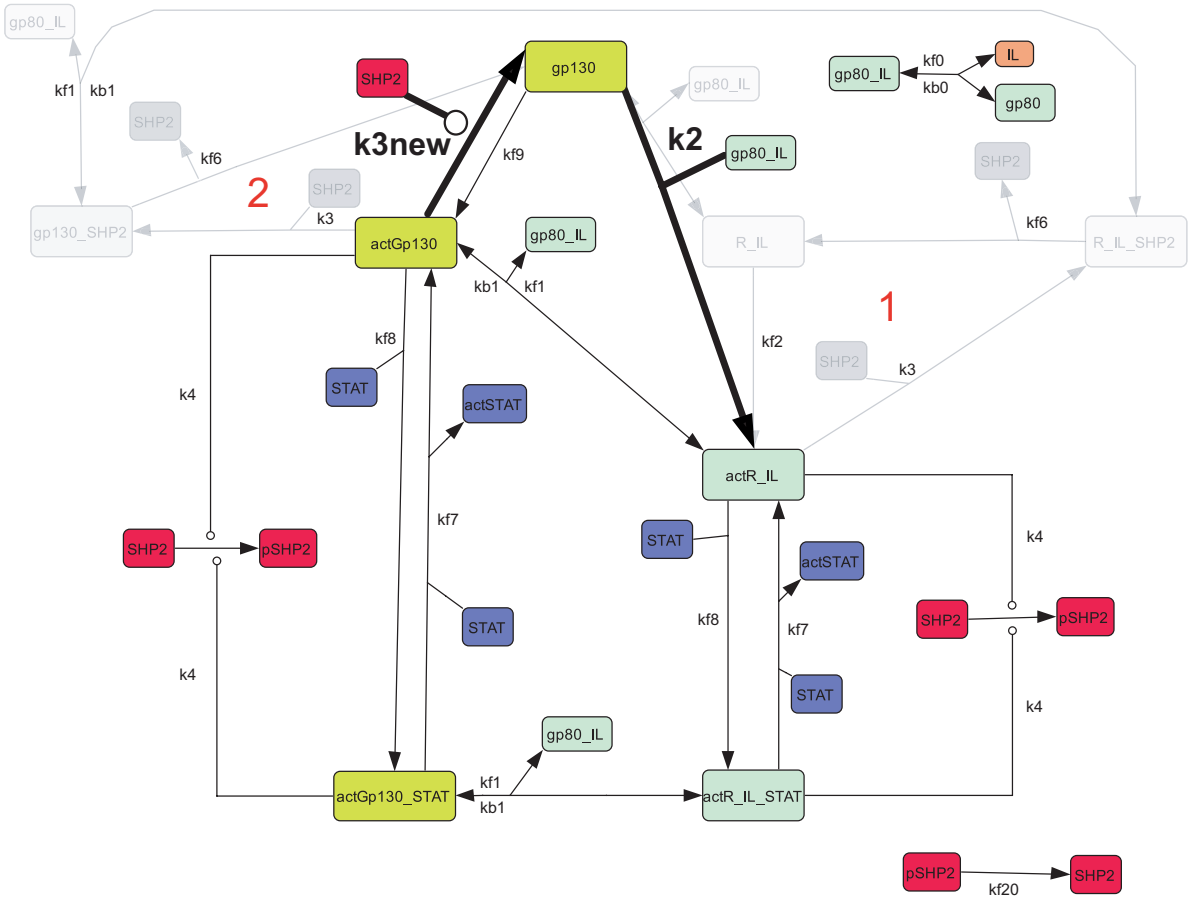


Figure S5: Graphical representation of model $M_4$. The same notation as in the previous figures is used. Two major simplification lead from $M_3$ to $M_4$. First, we assume that in the IL-6-induced part of the model, SHP2 is not able to inactivate the IL-6-bound activated receptor. Consequently, we have removed this part from the model (see model part marked with a red 1). By this we can model the IL-6-induced receptor activation with only one reaction (bold reaction arrow with kinetic constant k2). Second, we model the SHP2-induced inactivation of the IL-6-free activated receptor (actGp130) with a pseudo first order reaction (bold reaction with kinetic constant k3new). By this we can neglect the complex formation between SHP2 and actGp130 (grayed part labeled with red 2). A mathematical representation of this model is given in Table S5.

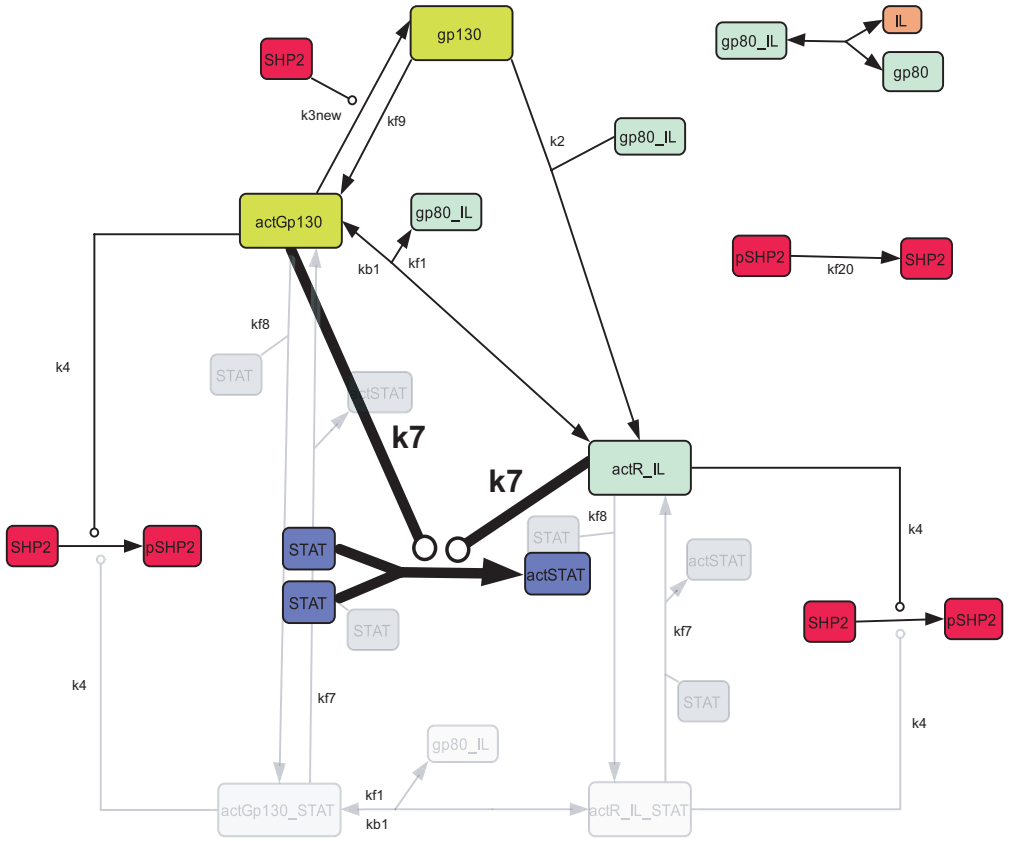


Figure S6: Graphical representation of model $M_5$. The same notation as in the previous figures is used. In analogy to previous changes, we neglect the complex formation between activated receptor and STAT (see grayed parts) and replace this part with a pseudo first order reaction (see bold reaction arrows with kinetic constant k7). A mathematical representation of this model is given in Table S6.

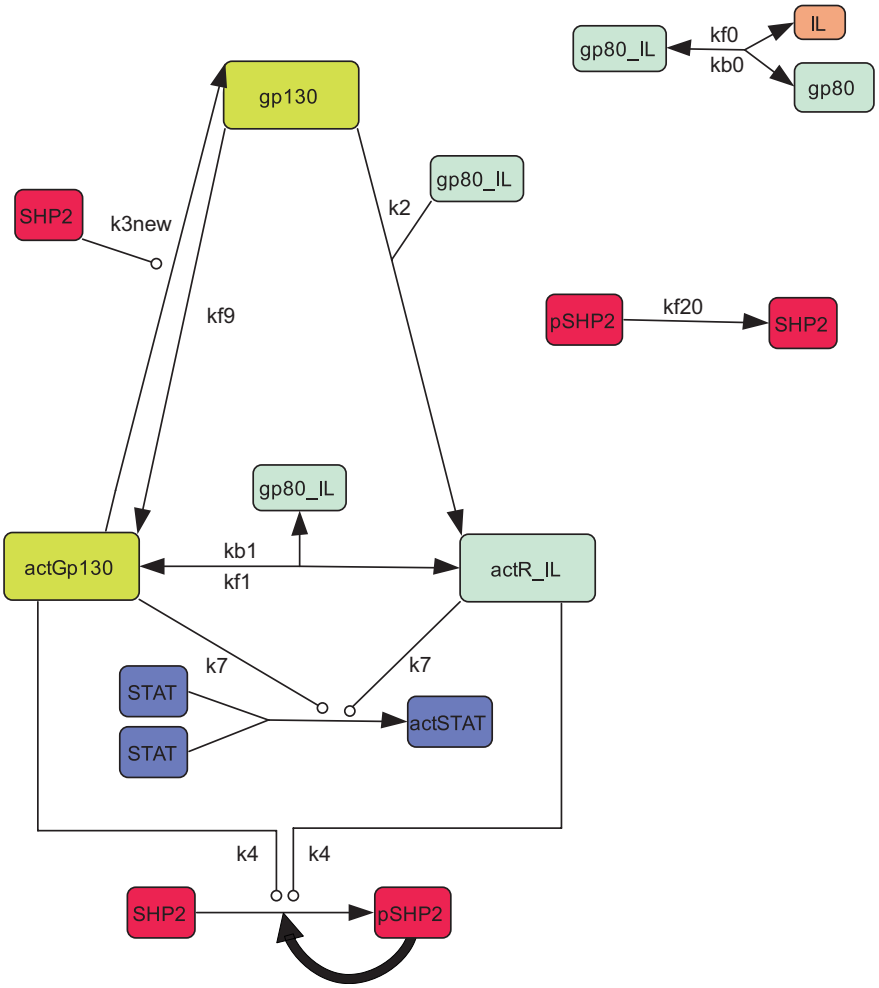


Figure S7: Graphical representation of model $M_6$. The same notation as in the previous figures is used. In contrast to $M_5$ we assume a positive feedback of pSHP2 on the phosphorylation of SHP2. This has been necessary to resolve discrepancies between model output $y_3$ and the pSHP2 data. A mathematical representation of this model is given in Table S7.

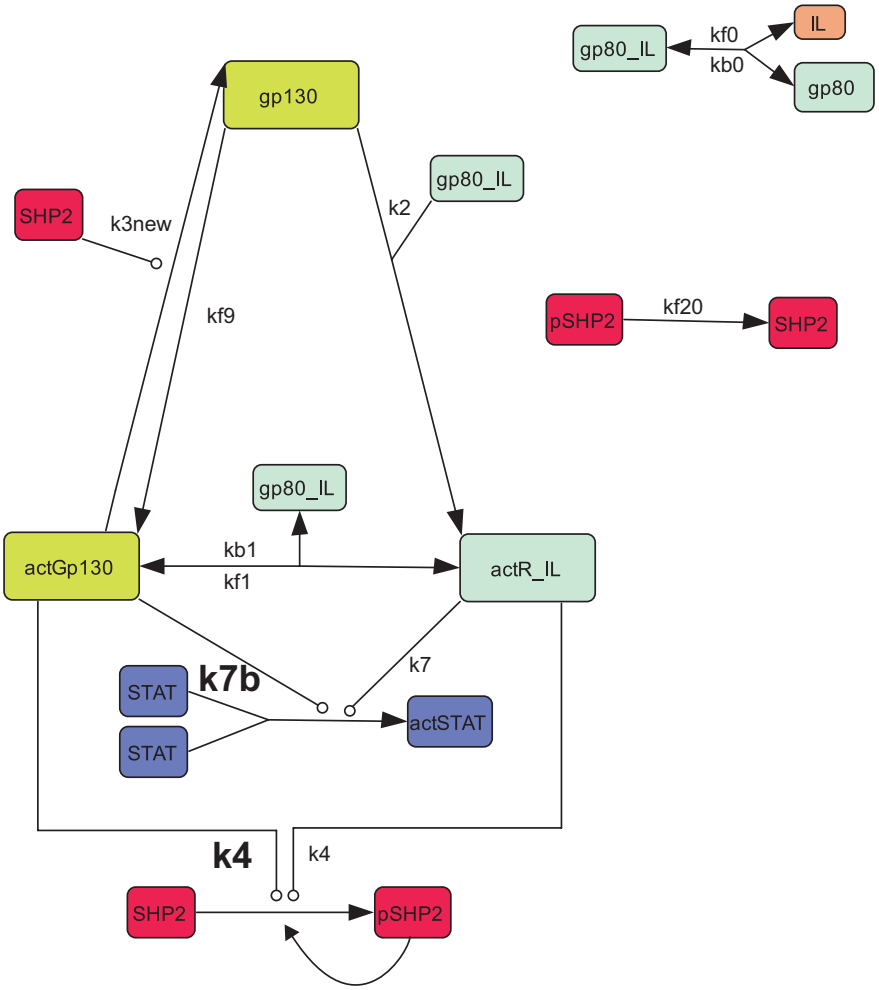


Figure S8: Graphical representation of model $M_7$. The same notation as in the previous figures is used. In contrast to $M_6$ we now assume that SHP2 (or STAT) are activated by the activated receptor species (actGp130 and actR_IL) via reactions with different kinetic constants. The changed kinetic constants are depicted in bold letters. A mathematical representation of this model is given in Table S8.

Table S1: Variables, initial values (in nM), and model equations of $M_0$. For a graphical representation see Figure S1.

| Variables | Descrption | Initial values | Differential equations | Rate equations |
|---|---|---|---|---|
| $x_1$ | R | 1.32 | $\dot{x}_1 = -v_1 - v_9 + v_{13}$ | $v_1 = kf1 \cdot x_1 \cdot \text{IL} - kb1 \cdot x_5$ |
| $x_2 \rightarrow u$ | IL | 0.475 | | $v_2 = kf2 \cdot x_5$ |
| $x_3$ | SHP2 | 222.36 | $\dot{x}_3 = -v_3 + v_6 + v_{10} + v_{13} + v_{20}$ | $v_3 = kf3 \cdot x_6 \cdot x_3 - kb3 \cdot x_7$ |
| $x_4$ | STAT | 108.08 | $\dot{x}_4 = -v_8 - v_{15}$ | $v_4 = kf4 \cdot x_7$ |
| $x_5$ | R_IL | 0 | $\dot{x}_5 = +v_1 - v_2 + v_6$ | $v_5 = kf5 \cdot x_7 - kb5 \cdot x_{14}$ |
| $x_6$ | actR_IL | 0 | $\dot{x}_6 = +v_2 - v_3 + v_4 + v_7 - v_8 + v_{16}$ | $v_6 = kf6 \cdot x_{14}$ |
| $x_7$ | actR_IL_SHP2 | 0 | $\dot{x}_7 = +v_3 - v_4 - v_5 + v_{17}$ | $v_7 = kf7 \cdot x_{12}$ |
| $x_8$ | pSHP2 | 0 | $\dot{x}_8 = +v_4 + v_{11} - v_{20}$ | $v_8 = kf8 \cdot x_6 \cdot x_4$ |
| $x_9$ | actR | 0 | $\dot{x}_9 = +v_9 + v_{10} + v_{11} + v_{14} - v_{15} - v_{16}$ | $v_9 = kf9 \cdot x_1$ |
| $x_{10}$ | actR_SHP2 | 0 | $\dot{x}_{10} = -v_{10} - v_{11} + v_{12} - v_{17}$ | $v_{10} = kb10 \cdot x_{10} - kf10 \cdot x_3 \cdot x_9$ |
| $x_{11}$ | actR_STAT | 0 | $\dot{x}_{11} = -v_{14} + v_{15} - v_{19}$ | $v_{11} = kf11 \cdot x_{10}$ |
| $x_{12}$ | actR_IL_STAT | 0 | $\dot{x}_{12} = -v_7 + v_8 + v_{19}$ | $v_{12} = kb12 \cdot x_{15} - kf12 \cdot x_{10}$ |
| $x_{13}$ | actSTAT | 0 | $\dot{x}_{13} = +v_7 + v_{14}$ | $v_{13} = kf13 \cdot x_{15}$ |
| $x_{14}$ | R_IL_SHP2 | 0 | $\dot{x}_{14} = +v_5 - v_6 + v_{18}$ | $v_{14} = kf14 \cdot x_{11}$ |
| $x_{15}$ | R_SHP2 | 0 | $\dot{x}_{15} = -v_{12} - v_{13} - v_{18}$ | $v_{15} = kf15 \cdot x_9 \cdot x_4$ |
| | | | | $v_{16} = kf1 \cdot x_9 \cdot \text{IL} - kb1 \cdot x_6$ |
| | | | | $v_{17} = kf1 \cdot x_{10} \cdot \text{IL} - kb1 \cdot x_7$ |
| | | | | $v_{18} = kf1 \cdot x_{15} \cdot \text{IL} - kb1 \cdot x_{14}$ |
| | | | | $v_{19} = kf1 \cdot x_{11} \cdot \text{IL} - kb1 \cdot x_{12}$ |
| | | | | $v_{20} = kf20 \cdot x_8$ |

Table S2: Variables, initial values (in nM), and model equations of $M_1$. For a graphical representation see Figure S2.

| Variables | Description | Initial values | Differential equations | Rate equations |
|---|---|---|---|---|
| $x_1$ | gp130 | 1.32 | $\dot{x}_1 = -v_1 - v_9 + v_{13}$ | $v_1 = kf1 \cdot x_1 \cdot x_{17} - kb1 \cdot x_5$ |
| $x_2 \rightarrow u$ | IL | 0.475 | | $v_2 = kf2 \cdot x_5$ |
| $x_3$ | SHP2 | 222.36 | $\dot{x}_3 = -v_3 + v_6 + v_{10} + v_{13} + v_{20}$ | $v_3 = kf3 \cdot x_6 \cdot x_3 - kb3 \cdot x_7$ |
| $x_4$ | STAT | 108.08 | $\dot{x}_4 = -v_8 - v_{15}$ | $v_4 = kf4 \cdot x_7$ |
| $x_5$ | R_IL | 0 | $\dot{x}_5 = +v_1 - v_2 + v_6$ | $v_5 = kf5 \cdot x_7 - kb5 \cdot x_{14}$ |
| $x_6$ | actR_IL | 0 | $\dot{x}_6 = +v_2 - v_3 + v_4 + v_7 - v_8 + v_{16}$ | $v_6 = kf6 \cdot x_{14}$ |
| $x_7$ | actR_IL_SHP2 | 0 | $\dot{x}_7 = +v_3 - v_4 - v_5 + v_{17}$ | $v_7 = kf7 \cdot x_{12}$ |
| $x_8$ | pSHP2 | 0 | $\dot{x}_8 = +v_4 + v_{11} - v_{20}$ | $v_8 = kf8 \cdot x_6 \cdot x_4$ |
| $x_9$ | actGp130 | 0 | $\dot{x}_9 = +v_9 + v_{10} + v_{11} + v_{14} - v_{15} - v_{16}$ | $v_9 = kf9 \cdot x_1$ |
| $x_{10}$ | actGp130_SHP2 | 0 | $\dot{x}_{10} = -v_{10} - v_{11} + v_{12} - v_{17}$ | $v_{10} = kb10 \cdot x_{10} - kf10 \cdot x_3 \cdot x_9$ |
| $x_{11}$ | actGp130_STAT | 0 | $\dot{x}_{11} = -v_{14} + v_{15} - v_{19}$ | $v_{11} = kf11 \cdot x_{10}$ |
| $x_{12}$ | actR_IL_STAT | 0 | $\dot{x}_{12} = -v_7 + v_8 + v_{19}$ | $v_{12} = kb12 \cdot x_{15} - kf12 \cdot x_{10}$ |
| $x_{13}$ | actSTAT | 0 | $\dot{x}_{13} = +v_7 + v_{14}$ | $v_{13} = kf13 \cdot x_{15}$ |
| $x_{14}$ | R_IL_SHP2 | 0 | $\dot{x}_{14} = +v_5 - v_6 + v_{18}$ | $v_{14} = kf14 \cdot x_{11}$ |
| $x_{15}$ | gp130_SHP2 | 0 | $\dot{x}_{15} = -v_{12} - v_{13} - v_{18}$ | $v_{15} = kf15 \cdot x_9 \cdot x_4$ |
| $x_{16}$ | gp80 | 133.10 | $\dot{x}_{16} = -v_{21}$ | $v_{16} = kf1 \cdot x_9 \cdot x_{17} - kb1 \cdot x_6$ |
| $x_{17}$ | gp80_IL | 0 | $\dot{x}_{17} = -v_1 - v_{16} - v_{17} - v_{18} - v_{19} + v_{21}$ | $v_{17} = kf1 \cdot x_{10} \cdot x_{17} - kb1 \cdot x_7$ |
| | | | | $v_{18} = kf1 \cdot x_{15} \cdot x_{17} - kb1 \cdot x_{14}$ |
| | | | | $v_{19} = kf1 \cdot x_{11} \cdot x_{17} - kb1 \cdot x_{12}$ |
| | | | | $v_{20} = kf20 \cdot x_8$ |
| | | | | $v_{21} = kf0 \cdot \mathrm{IL} \cdot x_{16} - kb0 \cdot x_{17}$ |

Table S3: Variables, initial values (in nM), and model equations of $M_2$. For a graphical representation see Figure S3.

| Variables | Description | Initial values | Differential equations | Rate equations |
|---|---|---|---|---|
| $x_1$ | gp130 | 1.32 | $\dot{x}_1 = -v_1 - v_9 + v_{13}$ | $v_1 = kf1 \cdot x_1 \cdot x_{17} - kb1 \cdot x_5$ |
| $x_2 \rightarrow u$ | IL | 0.475 | | $v_2 = kf2 \cdot x_5$ |
| $x_3$ | SHP2 | 222.36 | $\dot{x}_3 = -v_3 + v_6 + v_{10} + v_{13} + v_{20}$ | $v_3 = kf3 \cdot x_6 \cdot x_3 - kb3 \cdot x_7$ |
| $x_4$ | STAT | 108.08 | $\dot{x}_4 = -v_8 - v_{15}$ | $v_4 = kf4 \cdot x_7$ |
| $x_5$ | R_IL | 0 | $\dot{x}_5 = +v_1 - v_2 + v_6$ | $v_5 = kf5 \cdot x_7 - kb5 \cdot x_{14}$ |
| $x_6$ | actR_IL | 0 | $\dot{x}_6 = +v_2 - v_3 + v_4 + v_7 - v_8 + v_{16}$ | $v_6 = kf6 \cdot x_{14}$ |
| $x_7$ | actR_IL_SHP2 | 0 | $\dot{x}_7 = +v_3 - v_4 - v_5 + v_{17}$ | $v_7 = kf7 \cdot x_{12}$ |
| $x_8$ | pSHP2 | 0 | $\dot{x}_8 = +v_4 + v_{11} - v_{20}$ | $v_8 = kf8 \cdot x_6 \cdot x_4$ |
| $x_9$ | actGp130 | 0 | $\dot{x}_9 = +v_9 + v_{10} + v_{11} + v_{14} - v_{15} - v_{16}$ | $v_9 = kf9 \cdot x_1$ |
| $x_{10}$ | actGp130_SHP2 | 0 | $\dot{x}_{10} = -v_{10} - v_{11} + v_{12} - v_{17}$ | $v_{10} = kb3 \cdot x_{10} - kf3 \cdot x_3 \cdot x_9$ |
| $x_{11}$ | actGp130_STAT | 0 | $\dot{x}_{11} = -v_{14} + v_{15} - v_{19}$ | $v_{11} = kf4 \cdot x_{10}$ |
| $x_{12}$ | actR_IL_STAT | 0 | $\dot{x}_{12} = -v_7 + v_8 + v_{19}$ | $v_{12} = kb5 \cdot x_{15} - kf5 \cdot x_{10}$ |
| $x_{13}$ | actSTAT | 0 | $\dot{x}_{13} = +v_7 + v_{14}$ | $v_{13} = kf6 \cdot x_{15}$ |
| $x_{14}$ | R_IL_SHP2 | 0 | $\dot{x}_{14} = +v_5 - v_6 + v_{18}$ | $v_{14} = kf7 \cdot x_{11}$ |
| $x_{15}$ | gp130_SHP2 | 0 | $\dot{x}_{15} = -v_{12} - v_{13} - v_{18}$ | $v_{15} = kf8 \cdot x_9 \cdot x_4$ |
| $x_{16}$ | gp80 | 133.10 | $\dot{x}_{16} = -v_{21}$ | $v_{16} = kf1 \cdot x_9 \cdot x_{17} - kb1 \cdot x_6$ |
| $x_{17}$ | gp80_IL | 0 | $\dot{x}_{17} = -v_1 - v_{16} - v_{17} - v_{18} - v_{19} + v_{21}$ | $v_{17} = kf1 \cdot x_{10} \cdot x_{17} - kb1 \cdot x_7$ |
| | | | | $v_{18} = kf1 \cdot x_{15} \cdot x_{17} - kb1 \cdot x_{14}$ |
| | | | | $v_{19} = kf1 \cdot x_{11} \cdot x_{17} - kb1 \cdot x_{12}$ |
| | | | | $v_{20} = kf20 \cdot x_8$ |
| | | | | $v_{21} = kf0 \cdot \mathrm{IL} \cdot x_{16} - kb0 \cdot x_{17}$ |

Table S4: Variables, initial values (in nM), and model equations of $M_3$. For a graphical representation see Figure S4.

| Variables | Description | Initial values | Differential equations | Rate equations |
|---|---|---|---|---|
| $x_1$ | gp130 | 1.32 | $\dot{x}_1 = -v_1 - v_5 + v_6$ | $v_1 = kf1 \cdot x_1 \cdot x_{17} - kb1 \cdot x_5$ |
| $x_2 \rightarrow u$ | IL | 0.475 | | $v_2 = kf2 \cdot x_5$ |
| $x_3$ | SHP2 | 222.36 | $\dot{x}_3 = +v_3 + v_6 + v_{11} - v_{15} - v_{16} - v_{17} - v_{18}$ | $v_3 = kf6 \cdot x_{14}$ |
| $x_4$ | STAT | 216.17 | $\dot{x}_4 = -v_4 - v_7 - v_{13} - v_{14}$ | $v_4 = kf8 \cdot x_6 \cdot x_4$ |
| $x_5$ | R_IL | 0 | $\dot{x}_5 = +v_1 - v_2 + v_3$ | $v_5 = kf9 \cdot x_1$ |
| $x_6$ | actR_IL | 0 | $\dot{x}_6 = +v_2 - v_4 + v_8 + v_{13} - v_{18}$ | $v_6 = kf6 \cdot x_{15}$ |
| $x_8$ | pSHP2 | 0 | $\dot{x}_8 = -v_{11} + v_{15} + v_{17}$ | $v_7 = kf8 \cdot x_9 \cdot x_4$ |
| $x_9$ | actGp130 | 0 | $\dot{x}_9 = +v_5 - v_7 - v_8 + v_{14} - v_{16}$ | $v_8 = kf1 \cdot x_9 \cdot x_{17} - kb1 \cdot x_6$ |
| $x_{11}$ | actGp130_STAT | 0 | $\dot{x}_{11} = +v_7 - v_{10} - v_{14}$ | $v_9 = kf1 \cdot x_{15} \cdot x_{17} - kb1 \cdot x_{14}$ |
| $x_{12}$ | actR_IL_STAT | 0 | $\dot{x}_{12} = +v_4 + v_{10} - v_{13}$ | $v_{10} = kf1 \cdot x_{11} \cdot x_{17} - kb1 \cdot x_{12}$ |
| $x_{13}$ | actSTAT | 0 | $\dot{x}_{13} = +v_{13} + v_{14}$ | $v_{11} = kf20 \cdot x_8$ |
| $x_{14}$ | R_IL_SHP2 | 0 | $\dot{x}_{14} = -v_3 + v_9 + v_{18}$ | $v_{12} = kf0 \cdot \mathrm{IL} \cdot x_{16} - kb0 \cdot x_{17}$ |
| $x_{15}$ | gp130_SHP2 | 0 | $\dot{x}_{15} = -v_6 - v_9 + v_{16}$ | $v_{13} = x_{12} \cdot x_4 \cdot kf7$ |
| $x_{16}$ | gp80 | 133.10 | $\dot{x}_{16} = -v_{12}$ | $v_{14} = x_{11} \cdot x_4 \cdot kf7$ |
| $x_{15}$ | gp80_IL | 0 | $\dot{x}_{17} = -v_1 - v_8 - v_9 - v_{10} + v_{12}$ | $v_{15} = x_3 \cdot x_9 \cdot k4 + x_3 \cdot x_{11} \cdot k4$ |
| | | | | $v_{16} = k3 \cdot x_9 \cdot x_3$ |
| | | | | $v_{17} = k4 \cdot x_3 \cdot x_6 + k4 \cdot x_3 \cdot x_{12}$ |
| | | | | $v_{18} = k3 \cdot x_6 \cdot x_3$ |

Table S5: Variables, initial values (in nM), and model equations of $M_4$. For a graphical representation see Figure S5.

| Variables | Description | Initial values | Differential equations | Rate equations |
|---|---|---|---|---|
| $x_1$ | gp130 | 1.32 | $\dot{x}_1 = -v_2 - v_{12} + v_{13}$ | $v_1 = kf8 \cdot x_6 \cdot x_4$ |
| $x_2 \rightarrow u$ | IL | 0.475 | | $v_2 = kf9 \cdot x_1$ |
| $x_3$ | SHP2 | 222.36 | $\dot{x}_3 = +v_6 - v_{10} - v_{11}$ | $v_3 = kf8 \cdot x_9 \cdot x_4$ |
| $x_4$ | STAT | 216.17 | $\dot{x}_4 = -v_1 - v_3 - v_8 - v_9$ | $v_4 = kf1 \cdot x_9 \cdot x_{17} - kb1 \cdot x_6$ |
| $x_6$ | actR_IL | 0 | $\dot{x}_6 = -v_1 + v_4 + v_8 + v_{12}$ | $v_5 = kf1 \cdot x_{11} \cdot x_{17} - kb1 \cdot x_{12}$ |
| $x_8$ | pSHP2 | 0 | $\dot{x}_8 = -v_6 + v_{10} + v_{11}$ | $v_6 = kf20 \cdot x_8$ |
| $x_9$ | actGp130 | 0 | $\dot{x}_9 = +v_2 - v_3 - v_4 + v_9 - v_{13}$ | $v_7 = kf0 \cdot \mathrm{IL} \cdot x_{16} - kb0 \cdot x_{17}$ |
| $x_{11}$ | actGp130_STAT | 0 | $\dot{x}_{11} = +v_3 - v_5 - v_9$ | $v_8 = x_{12} \cdot x_4 \cdot kf7$ |
| $x_{12}$ | actR_IL_STAT | 0 | $\dot{x}_{12} = +v_1 + v_5 - v_8$ | $v_9 = x_{11} \cdot x_4 \cdot kf7$ |
| $x_{13}$ | actSTAT | 0 | $\dot{x}_{13} = +v_8 + v_9$ | $v_{10} = x_3 \cdot x_9 \cdot k4 + x_3 \cdot x_{11} \cdot k4$ |
| $x_{16}$ | gp80 | 133.10 | $\dot{x}_{16} = -v_7$ | $v_{11} = k4 \cdot x_3 \cdot x_6 + k4 \cdot x_3 \cdot x_{12}$ |
| $x_{17}$ | gp80_IL | 0 | $\dot{x}_{17} = -v_4 - v_5 + v_7 - v_{12}$ | $v_{12} = k2 \cdot x_1 \cdot x_{17}$ |
| | | | | $v_{13} = k3new \cdot x_9 \cdot x_3$ |

Table S6: Variables, initial values (in nM), and model equations of $M_5$. For a graphical representation see Figure S6.

| Variables | Description | $x_i^{\text{Exp 1}}(0)$ | $x_i^{\text{Exp 2}}(0)$ | Differential equations | Rate equations |
|---|---|---|---|---|---|
| $x_2 \rightarrow u$ | IL | 0.48 | 0.48 | | $v_1 = kf9 \cdot (gp130Total - x_6 - x_9)$ |
| $x_3$ | SHP2 | 222.36 | 128.27 | $\dot{x}_3 = +v_3 - v_5$ | $v_2 = kf1 \cdot x_9 \cdot x_{17} - kb1 \cdot x_6$ |
| $x_4$ | STAT | 216.17 | 205.50 | $\dot{x}_4 = -2.0 \cdot v_6$ | $v_3 = kf20 \cdot x_8$ |
| $x_6$ | actR_IL | 0.00 | 0.00 | $\dot{x}_6 = +v_2 + v_8$ | $v_4 = kf0 \cdot IL \cdot x_{16} - kb0 \cdot x_{17}$ |
| $x_8$ | pSHP2 | 0.00 | 1.30 | $\dot{x}_8 = -v_3 + v_5$ | $v_5 = x_3 \cdot x_9 \cdot k4 + x_3 \cdot x_6 \cdot k4$ |
| $x_9$ | actGp130 | 0.00 | 0.00 | $\dot{x}_9 = +v_1 - v_2 - v_7$ | $v_6 = k7 \cdot x_4^2 \cdot x_9 + k7 \cdot x_4^2 \cdot x_6$ |
| $x_{13}$ | actSTAT | 0.00 | 5.35 | $\dot{x}_{13} = +v_6$ | $v_7 = k3new \cdot x_9 \cdot x_3$ |
| $x_{16}$ | gp80 | 133.10 | 133.10 | $\dot{x}_{16} = -v_4$ | $v_8 = k2 \cdot (gp130Total - x_6 - x_9) \cdot x_{17}$ |
| $x_{17}$ | gp80_IL | 0.00 | 0.00 | $\dot{x}_{17} = -v_2 + v_4 - v_8$ | |

Table S7: Variables, initial values (in nM), and model equations of $M_6$. For a graphical representation see Figure S7.

| Variables | Description | $x_i^{\text{Exp 1}}(0)$ | $x_i^{\text{Exp 2}}(0)$ | Differential equations | Rate equations |
|---|---|---|---|---|---|
| $x_2 \rightarrow u$ | IL | 0.48 | 0.48 | | $v_1 = kf9 \cdot (gp130Total - x_6 - x_9)$ |
| $x_3$ | SHP2 | 222.36 | 128.27 | $\dot{x}_3 = +v_3 - v_5$ | $v_2 = kf1 \cdot x_9 \cdot x_{17} - kb1 \cdot x_6$ |
| $x_4$ | STAT | 216.17 | 205.50 | $\dot{x}_4 = -2.0 \cdot v_6$ | $v_3 = kf20 \cdot x_8$ |
| $x_6$ | actR_IL | 0.00 | 0.00 | $\dot{x}_6 = +v_2 + v_8$ | $v_4 = kf0 \cdot IL \cdot x_{16} - kb0 \cdot x_{17}$ |
| $x_8$ | pSHP2 | 0.00 | 1.30 | $\dot{x}_8 = -v_3 + v_5$ | $v_5 = x_3 \cdot x_9 \cdot k4 \cdot (1\text{nM} + x_8) + x_3 \cdot x_6 \cdot k4 \cdot (1\text{nM} + x_8)$ |
| $x_9$ | actGp130 | 0.00 | 0.00 | $\dot{x}_9 = +v_1 - v_2 - v_7$ | $v_6 = k7 \cdot x_4^2 \cdot x_9 + k7 \cdot x_4^2 \cdot x_6$ |
| $x_{13}$ | actSTAT | 0.00 | 5.35 | $\dot{x}_{13} = +v_6$ | $v_7 = k3new \cdot x_9 \cdot x_3$ |
| $x_{16}$ | gp80 | 133.10 | 133.10 | $\dot{x}_{16} = -v_4$ | $v_8 = k2 \cdot (gp130Total - x_6 - x_9) \cdot x_{17}$ |
| $x_{17}$ | gp80_IL | 0.00 | 0.00 | $\dot{x}_{17} = -v_2 + v_4 - v_8$ | |

Table S8: Variables, initial values (in nM), and model equations of $M_7$. For a graphical representation see Figure S8.

| Variables | Description | $x_i^{\text{Exp 1}}(0)$ | $x_i^{\text{Exp 2}}(0)$ | Differential equations | Rate equations |
|---|---|---|---|---|---|
| $x_2 \rightarrow u$ | IL | 0.95 | 0.95 | | $v_1 = kf9 \cdot (gp130Total - x_6 - x_9)$ |
| $x_3$ | SHP2 | 222.36 | 128.27 | $\dot{x}_3 = +v_3 - v_5$ | $v_2 = kf1 \cdot x_9 \cdot x_{17} - kb1 \cdot x_6$ |
| $x_4$ | STAT | 216.17 | 205.50 | $\dot{x}_4 = -2.0 \cdot v_6$ | $v_3 = kf20 \cdot x_8$ |
| $x_6$ | actR_IL | 0.00 | 0.00 | $\dot{x}_6 = +v_2 + v_8$ | $v_4 = kf0 \cdot IL \cdot x_{16} - kb0 \cdot x_{17}$ |
| $x_8$ | pSHP2 | 0.00 | 1.30 | $\dot{x}_8 = -v_3 + v_5$ | $v_5 = x_3 \cdot x_9 \cdot k4b + x_3 \cdot x_9 \cdot k4b \cdot x_8 + x_3 \cdot x_6 \cdot k4 + x_3 \cdot x_6 \cdot k4 \cdot x_8$ |
| $x_9$ | actGp130 | 0.00 | 0.00 | $\dot{x}_9 = +v_1 - v_2 - v_7$ | $v_6 = k7b \cdot x_4^2 \cdot x_9 + k7 \cdot x_4^2 \cdot x_6$ |
| $x_{13}$ | actSTAT | 0.00 | 5.35 | $\dot{x}_{13} = +v_6$ | $v_7 = k3new \cdot x_9 \cdot x_3$ |
| $x_{16}$ | gp80 | 133.10 | 133.10 | $\dot{x}_{16} = -v_4$ | $v_8 = k2 \cdot (gp130Total - x_6 - x_9) \cdot x_{17}$ |
| $x_{17}$ | gp80_IL | 0.00 | 0.00 | $\dot{x}_{17} = -v_2 + v_4 - v_8$ | |

Table S9: Estimated parameters of models $M_0$ to $M_7$

| Model | Parameter values ($s^{-1}$ for first-order and $nM^{-1} \cdot s^{-1}$ for second-order rate constants) |
|---|---|
| $M_0$ | kb1 $= 0.21 \cdot 10^{-2}$, kb10 $= 1.3$, kb12 $= 0.21$, kb3 $= 0.12 \cdot 10^{4}$, kb5 $= 0.10 \cdot 10^{-5}$, kf1 $= 0.12 \cdot 10^{-1}$, kf10 $= 0.84 \cdot 10^{-3}$, kf11 $= 0.27 \cdot 10^{-1}$, kf12 $= 51.$, kf13 $= 0.20 \cdot 10^{-1}$, kf14 $= 0.13 \cdot 10^{-4}$, kf15 $= 0.11 \cdot 10^{-3}$, kf2 $= 0.36 \cdot 10^{-1}$, kf20 $= 0.94 \cdot 10^{-5}$, kf3 $= 44.$, kf4 $= 0.31 \cdot 10^{4}$, kf5 $= 52.$, kf6 $= 0.23 \cdot 10^{-2}$, kf7 $= 0.36 \cdot 10^{3}$, kf8 $= 67.$, kf9 $= 0.11 \cdot 10^{-4}$, scaleJAK $= 0.38 \cdot 10^{3}$ |
| $M_1$ | kb0 $= 0.36 \cdot 10^{-2}$, kb1 $= 3.3$, kb10 $= 0.10 \cdot 10^{5}$, kb12 $= 0.28$, kb3 $= 0.18 \cdot 10^{4}$, kb5 $= 0.17 \cdot 10^{-5}$, kf0 $= 0.86 \cdot 10^{-4}$, kf1 $= 0.42$, kf10 $= 0.61$, kf11 $= 0.61 \cdot 10^{4}$, kf12 $= 0.10 \cdot 10^{5}$, kf13 $= 0.49 \cdot 10^{-5}$, kf14 $= 0.54 \cdot 10^{-4}$, kf15 $= 0.10 \cdot 10^{-7}$, kf2 $= 0.18$, kf20 $= 0.17 \cdot 10^{-2}$, kf3 $= 49.$, kf4 $= 0.10 \cdot 10^{5}$, kf5 $= 0.21 \cdot 10^{3}$, kf6 $= 0.40 \cdot 10^{-5}$, kf7 $= 0.10 \cdot 10^{5}$, kf8 $= 0.10 \cdot 10^{3}$, kf9 $= 0.1 \cdot 10^{-5}$, scaleJAK $= 0.30 \cdot 10^{3}$ |
| $M_2$ | kb0 $= 0.32 \cdot 10^{-2}$, kb1 $= 0.89 \cdot 10^{3}$, kb3 $= 0.10 \cdot 10^{5}$, kb5 $= 0.36 \cdot 10^{-1}$, kf0 $= 0.86 \cdot 10^{-4}$, kf1 $= 20.$, kf2 $= 2.1$, kf20 $= 0.31 \cdot 10^{-2}$, kf3 $= 0.62$, kf4 $= 0.10 \cdot 10^{5}$, kf5 $= 0.97 \cdot 10^{3}$, kf6 $= 0.1 \cdot 10^{-5}$, kf7 $= 0.10 \cdot 10^{5}$, kf8 $= 0.42$, kf9 $= 0.1 \cdot 10^{-5}$, scaleJAK $= 0.15 \cdot 10^{3}$ |
| $M_3$ | k3 $= 3.5$, k4 $= 0.21 \cdot 10^{-1}$, kb0 $= 0.41 \cdot 10^{-2}$, kb1 $= 0.59$, kf0 $= 0.86 \cdot 10^{-4}$, kf1 $= 0.18$, kf2 $= 0.60 \cdot 10^{4}$, kf20 $= 0.14 \cdot 10^{-1}$, kf6 $= 0.94 \cdot 10^{3}$, kf7 $= 0.69 \cdot 10^{-2}$, kf8 $= 0.42$, kf9 $= 0.60 \cdot 10^{-4}$, scaleJAK $= 3.9$ |
| $M_4$ | k2 $= 0.28$, k3new $= 0.56 \cdot 10^{4}$, k4 $= 0.14 \cdot 10^{-1}$, kb0 $= 0.37 \cdot 10^{-2}$, kb1 $= 0.46$, kf0 $= 0.79 \cdot 10^{-4}$, kf1 $= 0.63 \cdot 10^{-6}$, kf20 $= 0.13 \cdot 10^{-1}$, kf7 $= 0.50 \cdot 10^{-2}$, kf8 $= 11.$, kf9 $= 0.40 \cdot 10^{-5}$, scaleJAK $= 2.7$ |
| $M_5$ | actGp130_0 $= 0.1 \cdot 10^{-4}$, k2 $= 0.27 \cdot 10^{-1}$, k3new $= 0.10 \cdot 10^{-8}$, k4 $= 0.92 \cdot 10^{-3}$, k7 $= 0.18 \cdot 10^{-4}$, kb0 $= 2.4$, kb1 $= 0.21$, kf0 $= 0.46 \cdot 10^{-2}$, kf1 $= 0.10 \cdot 10^{3}$, kf20 $= 0.42 \cdot 10^{-2}$, kf9 $= 0.10 \cdot 10^{-8}$, scaleJAK $= 2.4$, scaleJAK2 $= 0.35$ |
| $M_6$ | actGp130_0 $= 0.34 \cdot 10^{-4}$, k2 $= 0.52 \cdot 10^{-1}$, k3new $= 0.60 \cdot 10^{-8}$, k4 $= 1.0$, k7 $= 0.16 \cdot 10^{-4}$, kb0 $= 2.9$, kb1 $= 0.21$, kf0 $= 0.34 \cdot 10^{-2}$, kf1 $= 0.10 \cdot 10^{3}$, kf20 $= 0.10 \cdot 10^{3}$, kf9 $= 0.10 \cdot 10^{-8}$, scaleJAK $= 2.2$, scaleJAK2 $= 0.30$ |
| $M_7$ | actGp1300 $= 0.98 \cdot 10^{-5}$, k2 $= 0.11$, k3new $= 0.44 \cdot 10^{-7}$, k4 $= 0.84$, k4b $= 1.2$, k7 $= 0.21 \cdot 10^{-4}$, k7b $= 0.15 \cdot 10^{-5}$, kb0 $= 43.$, kb1 $= 1.5$, kf0 $= 0.26 \cdot 10^{-1}$, kf1 $= 0.11 \cdot 10^{5}$, kf20 $= 0.10 \cdot 10^{3}$, kf9 $= 0.10 \cdot 10^{-8}$, scaleJAK $= 2.2$, scaleJAK2 $= 0.30$ |

Table S10: Description of model variants of $M_5$. For a graphical representation see Figure 6

| Model | Modified for | Resulting model | Model changes |
|---|---|---|---|
| $M_5$ | pShp2 feedback replaced by positive feedback induced by activated STAT3 | $M_5$ with actSTAT feedback | $v_6 = x_9 \cdot k7 \cdot x_4^2 \cdot (1\text{nM} + x_{13}) + x_6 \cdot k7 \cdot x_4^2 \cdot (1\text{nM} + x_{13})$ |
| $M_5$ | pShp2 feedback replaced by positive feedback induced by IL-6-bound activated receptor | $M_5$ with actR feedback | $v_8 = k2 \cdot x_1 \cdot x_{17} \cdot (1\text{nM} + x_6)$ |

Table S11: Estimated parameter values for the model variants of $M_5$

| Model | Parameter values ($s^{-1}$ for first-order and $nM^{-1} \cdot s^{-1}$ for second-order rate constants) |
|---|---|
| $M_5$ with actSTAT feedback | actGp130_0 $= 0.1 \cdot 10^{-4}$, k2 $= 0.28 \cdot 10^{-1}$, k3new $= 0.10 \cdot 10^{-8}$, k4 $= 0.91 \cdot 10^{-3}$, k7 $= 0.87 \cdot 10^{-6}$, kb0 $= 2.5$, kb1 $= 0.20$, kf0 $= 0.47 \cdot 10^{-2}$, kf1 $= 0.10 \cdot 10^{3}$, kf20 $= 0.42 \cdot 10^{-2}$, kf9 $= 0.53 \cdot 10^{-8}$, scaleJAK $= 2.4$, scaleJAK2 $= 0.34$ |
| $M_5$ with actR feedback | actGp130_0 $= 0.1 \cdot 10^{-4}$, k2 $= 0.19 \cdot 10^{-1}$, k3new $= 0.10 \cdot 10^{-8}$, k4 $= 0.11 \cdot 10^{-2}$, k7 $= 0.19 \cdot 10^{-4}$, kb0 $= 2.6$, kb1 $= 0.17$, kf0 $= 0.53 \cdot 10^{-2}$, kf1 $= 0.10 \cdot 10^{3}$, kf20 $= 0.49 \cdot 10^{-2}$, kf9 $= 0.11 \cdot 10^{-8}$, scaleJAK $= 2.4$, scaleJAK2 $= 0.39$ |

Table S12: Description of model variants of $M_7$

| Model | Modified for | Resulting model | Model changes |
|---|---|---|---|
| $M_7$ | Shp2 feedback replaced by positive feedback induced by activated STAT3 | $M_7$ with actSTAT feedback | $v_5 = x_3 \cdot x_9 \cdot k4b + x_3 \cdot x_6 \cdot k4$, $v_6 = x_9 \cdot k7b \cdot x_4^2 \cdot (1\text{nM} + x_{13}) + x_6 \cdot k7 \cdot x_4^2 \cdot (1\text{nM} + x_{13})$ |
| $M_7$ | Shp2 feedback replaced by positive feedback induced by IL-6-bound activated receptor | $M_7$ with actR feedback | $v_5 = x_3 \cdot x_9 \cdot k4b + x_3 \cdot x_6 \cdot k4$, $v_6 = k7b\dot{x}_4^2 \cdot x_9 + k7 \cdot x_4^2 \cdot x_6$ |

Table S13: Estimated parameter values for the model variants of $M_7$

| Model | Parameter values ($s^{-1}$ for first-order and $nM^{-1} \cdot s^{-1}$ for second-order rate constants) |
|---|---|
| $M_7$ with actSTAT feedback | actGp130_0 $= 0.9$, k2 $= 0.48 \cdot 10^{-2}$, k3new $= 0.10 \cdot 10^{-8}$, k4 $= 0.60 \cdot 10^{-2}$, k4b $= 0.10 \cdot 10^{-8}$, k7 $= 0.22 \cdot 10^{-5}$, k7b $= 0.10 \cdot 10^{-8}$, kb0 $= 0.32 \cdot 10^{-1}$, kb1 $= 0.15 \cdot 10^{-2}$, kf0 $= 0.23 \cdot 10^{-3}$, kf1 $= 0.10 \cdot 10^{-8}$, kf20 $= 0.30 \cdot 10^{-2}$, kf9 $= 0.10 \cdot 10^{-8}$, scaleJAK $= 3.8$, scaleJAK2 $= 0.1$ |
| $M_7$ with actR feedback | actGp130_0 $= 0.9$, k2 $= 0.58 \cdot 10^{-2}$, k3new $= 0.10 \cdot 10^{-8}$, k4 $= 0.50 \cdot 10^{-2}$, k4b $= 0.10 \cdot 10^{-8}$, k7 $= 0.50 \cdot 10^{-4}$, k7b $= 0.45 \cdot 10^{-6}$, kb0 $= 0.42 \cdot 10^{-1}$, kb1 $= 0.18 \cdot 10^{-2}$, kf0 $= 0.26 \cdot 10^{-3}$, kf1 $= 0.10 \cdot 10^{-8}$, kf20 $= 0.25 \cdot 10^{-2}$, kf9 $= 0.10 \cdot 10^{-8}$, scaleJAK $= 3.0$, scaleJAK2 $= 0.1$ |

Table S14: Variables, initial values (in nM), and model equations of model $M_4$without actGp130. For a graphical representation see Figure 7

| Variables | Description | $x_i^{\text{Exp }1}(0)$ | $x_i^{\text{Exp }2}(0)$ | Differential equations | Rate equations |
|---|---|---|---|---|---|
| $x_1$ | gp130 | 1.32 | 1.24 | $\dot{x}_1 = -v_1$ | $v_1 = kf1 \cdot x_1 \cdot x_{17} - kb1 \cdot x_5$ |
| $x_2 \rightarrow u$ | IL | 0.48 | 0.48 | | $v_2 = kf2 \cdot x_5$ |
| $x_3$ | SHP2 | 222.36 | 129.57 | $\dot{x}_3 = +v_4 - v_7$ | $v_3 = kf8 \cdot x_6 \cdot x_4$ |
| $x_4$ | STAT | 216.17 | 216.17 | $\dot{x}_4 = -v_3 - v_6$ | $v_4 = kf20 \cdot x_8$ |
| $x_5$ | R_IL | 0.00 | 0.00 | $\dot{x}_5 = +v_1 - v_2 + v_8$ | $v_5 = kf0 \cdot IL \cdot x_{16} - kb0 \cdot x_{17}$ |
| $x_6$ | actR_IL | 0.00 | 0.00 | $\dot{x}_6 = +v_2 - v_3 + v_6 - v_8$ | $v_6 = x_{12} \cdot x_4 \cdot kf7$ |
| $x_8$ | pSHP2 | 0.00 | 0.00 | $\dot{x}_8 = -v_4 + v_7$ | $v_7 = k4 \cdot x_3 \cdot x_6 + k4 \cdot x_3 \cdot x_{12}$ |
| $x_{12}$ | actR_IL_STAT | 0.00 | 0.00 | $\dot{x}_{12} = +v_3 - v_6$ | $v_8 = k6 \cdot x_6 \cdot x_3$ |
| $x_{13}$ | actSTAT | 0.00 | 0.00 | $\dot{x}_{13} = +v_6$ | |
| $x_{16}$ | gp80 | 0.00 | 0.00 | $\dot{x}_{16} = -v_5$ | |
| $x_{17}$ | gp80_IL | 1.32 | 133.10 | $\dot{x}_{17} = -v_1 + v_5$ | |

Table S15: Description of model variants of $M_4$without actGp130

| Model | Modified for | Resulting model | Model changes |
|---|---|---|---|
| $M_4$ without actGp130 | positive feedback induced by phosphorylated SHP2 | $M_4$ without actGp130 pSHP2 feedback | $v_7 = x_3 \cdot x_6 \cdot k4 \cdot (1\text{nM} + x_8) + k4 \cdot x_3 \cdot x_{12} \cdot (1\text{nM} + x_8)$ |
| $M_4$ without actGp130 | positive feedback induced by activated STAT3 | $M_4$ without actGp130 actSTAT feedback | $v_6 = x_{12} \cdot x_4 \cdot kf7 \cdot (1\text{nM} + x_{13})$ |
| $M_4$ without actGp130 | positive feedback induced by IL-6-bound activated receptor | $M_4$ without actGp130 actR feedback | $v_2 = kf2 \cdot x_5 \cdot (1\text{nM} + x_6)$ |

Table S16: Estimated parameters of variants of $M_4$without actGp130

| Model description | Parameter values ($s^{-1}$ for first-order and $nM^{-1} \cdot s^{-1}$ for second-order rate constants) |
|---|---|
| $M_4$ without actGp130 | k4 $= 0.79 \cdot 10^{-2}$, k6 $= 0.1 \cdot 10^{-5}$, kb0 $= 0.10 \cdot 10^{6}$, kb1 $= 0.55 \cdot 10^{-1}$, kf0 $= 33.$, kf1 $= 0.10 \cdot 10^{4}$, kf2 $= 0.34 \cdot 10^{-3}$, kf20 $= 0.57 \cdot 10^{-2}$, kf7 $= 0.22 \cdot 10^{-1}$, kf8 $= 0.51 \cdot 10^{3}$, scaleJAK $= 20.$, scaleJAK2 $= 2.7$ |
| $M_4$ without actGp130 pSHP2 feedback | k4 $= 0.69 \cdot 10^{3}$, k6 $= 0.34 \cdot 10^{-4}$, kb0 $= 0.10 \cdot 10^{6}$, kb1 $= 0.57 \cdot 10^{-1}$, kf0 $= 34.$, kf1 $= 0.10 \cdot 10^{4}$, kf2 $= 0.34 \cdot 10^{-3}$, kf20 $= 0.75 \cdot 10^{4}$, kf7 $= 0.22 \cdot 10^{-1}$, kf8 $= 25.$, scaleJAK $= 20.$, scaleJAK2 $= 2.7$ |
| $M_4$ without actGp130 actSTAT feedback | k4 $= 0.76 \cdot 10^{-2}$, k6 $= 0.1 \cdot 10^{-5}$, kb0 $= 0.10 \cdot 10^{6}$, kb1 $= 0.55 \cdot 10^{-1}$, kf0 $= 33.$, kf1 $= 0.10 \cdot 10^{4}$, kf2 $= 0.35 \cdot 10^{-3}$, kf20 $= 0.53 \cdot 10^{-2}$, kf7 $= 36.$, kf8 $= 0.22 \cdot 10^{-1}$, scaleJAK $= 20.$, scaleJAK2 $= 2.7$ |
| $M_4$ without actGp130 actR feedback | k4 $= 0.79 \cdot 10^{-2}$, k6 $= 0.19 \cdot 10^{-5}$, kb0 $= 0.10 \cdot 10^{6}$, kb1 $= 0.55 \cdot 10^{-1}$, kf0 $= 33.$, kf1 $= 0.10 \cdot 10^{4}$, kf2 $= 0.34 \cdot 10^{-3}$, kf20 $= 0.56 \cdot 10^{-2}$, kf7 $= 0.22 \cdot 10^{-1}$, kf8 $= 0.96 \cdot 10^{3}$, scaleJAK $= 20.$, scaleJAK2 $= 2.7$ |

# Supplementary Information 2: Experimental validation of model assumption (4).

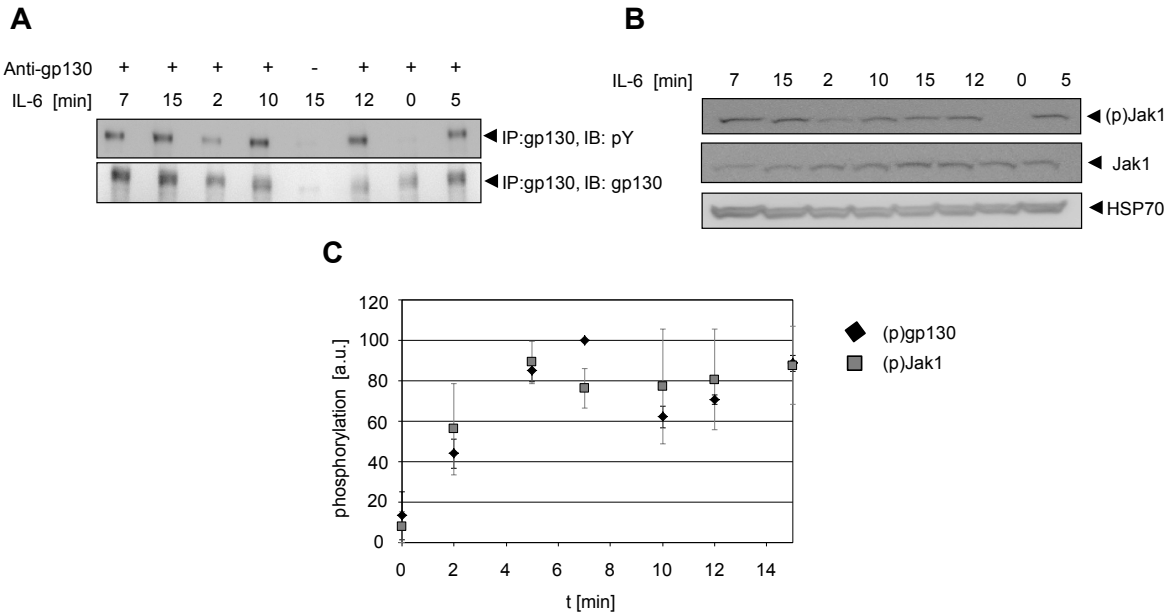


Figure S9: Validation of model assumption (2)

To validate the assumption (4) that the phosphorylation of Jak serves as indicator for receptor activation, HEK-gp80 cells were stimulated with IL-6 (0.95 nM) for up to 15 minutes. Phosphorylation of gp130 was analyzed by immunoprecipitation of gp130 and subsequent immunoblotting of the precipitates. Phosphorylated gp130 was then detected with specific antibodies against (p)Y. Detection of total gp130 served as loading control. For detection of phosphorylated Jak1 whole cell lysates were analyzed by immunoblotting using specific antibodies against (p)Jak1, Jak1 and HSP70. Detection of Jak1 and HSP70 served as loading control. Figure S9 A and B show representative immunoblot analysis. Maximum intensities have been set to 100 in every independent experiment. Figure S1 C presents mean $\pm$ SD of the densitometric analysis of $n = 3$ independent experiments.

IL-6-induced phosphorylation of gp130 and Jak1 do not differ in the first 15 minutes after stimulation, therefore, model assumption (4) is valid.

## Materials and Methods

### Immunoprecipitation

For immunoprecipitation lysates were incubated with $1\mu$g of antibody gp130 (M20, Santa Cruz technologies, Santa Cruz, CA) at $4°$C over night gp130 (M20). Subsequently, immunocomplexes were isolated using protein G dynabeads (Life technologies, Darmstadt, Germany) according to manufacturer‘s description. Phosphorylation of gp130 was detected with specific antibodies against (p)Y (pY99, Santa cruz technologies, Santa Cruz, CA, USA). The other immunoblots were performed as described in Material and Methods in the main text.

# Supplementary Information 3: Experimental validation of model assumption (11).

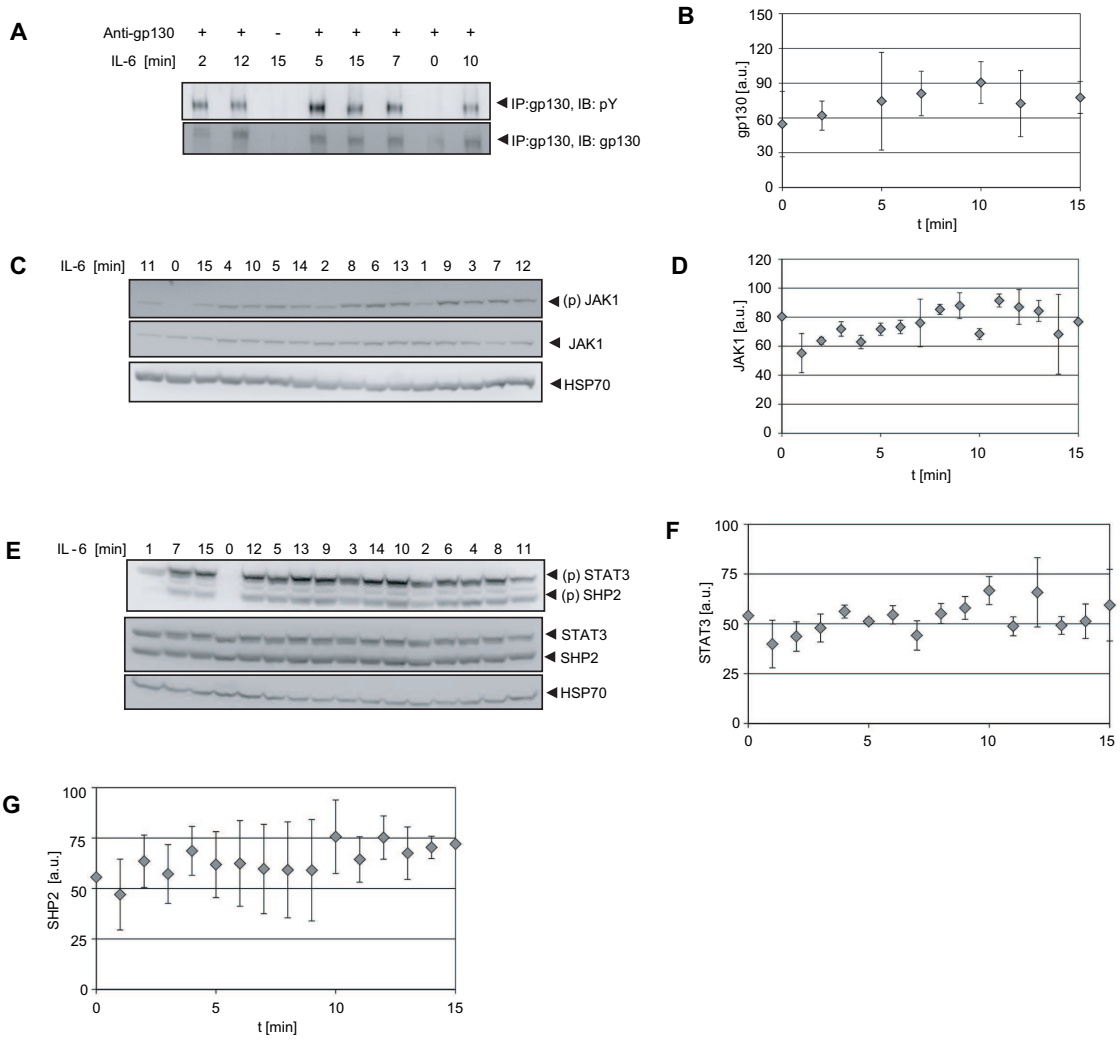


Figure S10: Validation of model assumption (11)

To validate model assumption (11) that the amounts of gp130, Jak1, STAT3 and SHP2 do not change in the first 15 minutes of IL-6 stimulation, HEK-gp130 cells were stimulated for up to 15 minutes with IL-6 (0,95 nM). gp130 was analyzed by immunoprecipitation of gp130 and subsequent immunoblotting of the precipitates, whereas (p)Jak1, Jak1, (p)STAT3, STAT3, (p)SHP2, SHP2, HSP70 were analyzed by immunoblotting aliquots of whole cell lysates. Detection of the phosphorylated species served as stimulation control. Detection of HSP70 served as loading control. Figure S10 A, C, and E present representative immunoblot analysis for gp130, Jak1 and STAT3/SHP2 respectively. Maximum intensities have been set to 100 in every independent experiment. Figure S10 B, D, F, and G present densitometric analysis of $n = 3$ independent experiments for gp130, Jak1, STAT3 and SHP2, respectively.

The amounts of unphosphorylated species gp130, Jak1, STAT3 and SHP2 do not change in the first 15 minutes after stimulation, therefore, model assumption (11) is valid.

# Supplementary Information 4: Experimental validation of model assumption (12).

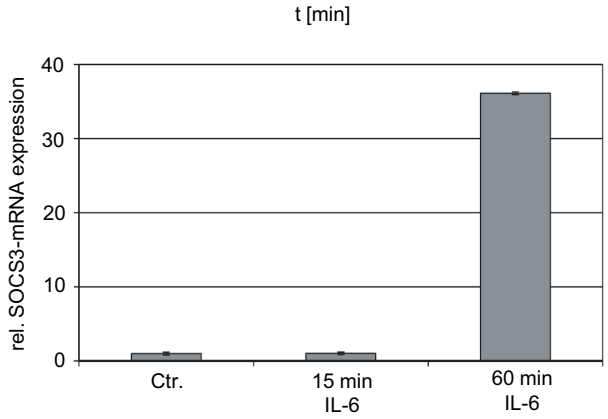


Figure S11: Validation of model assumption (12)

To validate model assumption (12) that SOCS3 is not expressed in the first 15 minutes after IL-6 stimulation, HEK-gp80 cells were stimulated for the indicated time periods with IL-6. After isolation of total RNA SOCS3 mRNA expression was analyzed by RT-qPCR. Figure S11 presents the mean $\pm$ SD of $n = 3$ independent experiments.

IL-6 does not induce the expression of SOCS3 mRNA within 15 minutes, whereas a 60 minute stimulation results in a strong synthesis of SOCS3 mRNA, therefore, model assumption (12) is valid.

## Materials and Methods

### Real time PCR (RT-qPCR)

Total RNA was isolated using the RNeasy Kit (Qiagen, Hilden,Germany) according to manufacturer's instructions. 500 ng of RNA was reverse transcribed into cDNA with Omniscript (Qiagen, Hilden, Germany) using random hexameric primers according to manufacturer's instructions. Taqman gene expression assays for human SOCS3 (Hs02330328_s1) and human HPRT: (Hs99999909_m1) were obtained from Applied Biosystems (Carlsbad, CA, USA) and PCR was performed using qPCR Mastermix plus (Eurogentec, Cologne, Germany). The PCR reaction was done in a final volume of 10 $\mu$l containing 2 $\mu$l cDNA and 1 $\mu$l Taqman gene expression assay solution. After denaturation for 15 minutes at $94^{\circ}$C amplification was performed in 40 cycles (15 s at $94^{\circ}$C, 60 s at $60^{\circ}$C) on a Rotorgene (Qiagen). The gene of interest and the housekeeping gene were amplified in duplicates. The quantification of gene expression was calculated using the Pfaffl method [1].

# Supplementary Information 5: Quantification of the concentration of gp130 and gp80.

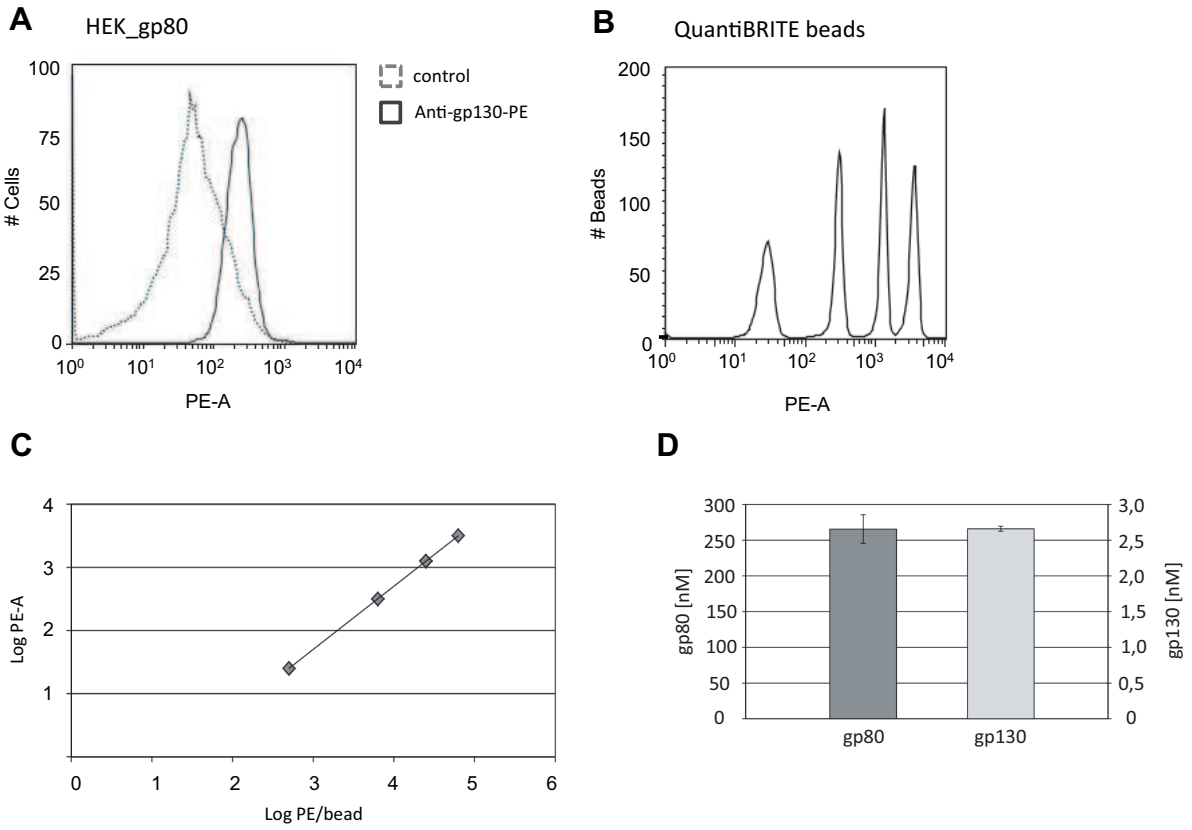


Figure S12: Quantification of receptor expression.

The amount of gp180 and gp130 was analyzed using a bead-based FACS assay. Figure S12 A shows the FACS analysis of HEK-gp80 cells with a directly PE (Phycoerithrin)-coupled antibody against gp130 (solid line). Control cells have not been stained with anti-gp130 antibodies (dashed line). Figure S12 B and C present the linear dependency of PE-fluorescence intensity with PE-amount on Quantibride beads. The amount of gp130 and gp80 on the cell membrane was calculated as 2.66 nM and 266 nM, respectively (see Figure S12 D).

## Materials and Methods

### Quantification of membrane-associated receptors

For quantification antibodies were directly coupled to PE using the phycolink PE conjugation kit (Prozyme, San Leandro, CA, USA) according to manufacturer‘s description. Antibody conjugates were purified using size exclusion chromatography and the ratio of PE/antibody was calculated by Lambert-Beer law. QuantiBRITE beads (BD, Heidelberg, Germany) were used to determine the amount of PE/cell. Cells and beads were analysed using the FACSCantoII (BD, Heidelberg, Germany). Data were analyzed using flowjo (Treestar, Ashland, OR, USA)

# Supplementary Information 6: Quantification of the concentration of STAT3, (p)STAT3, SHP2, and (p)SHP2.

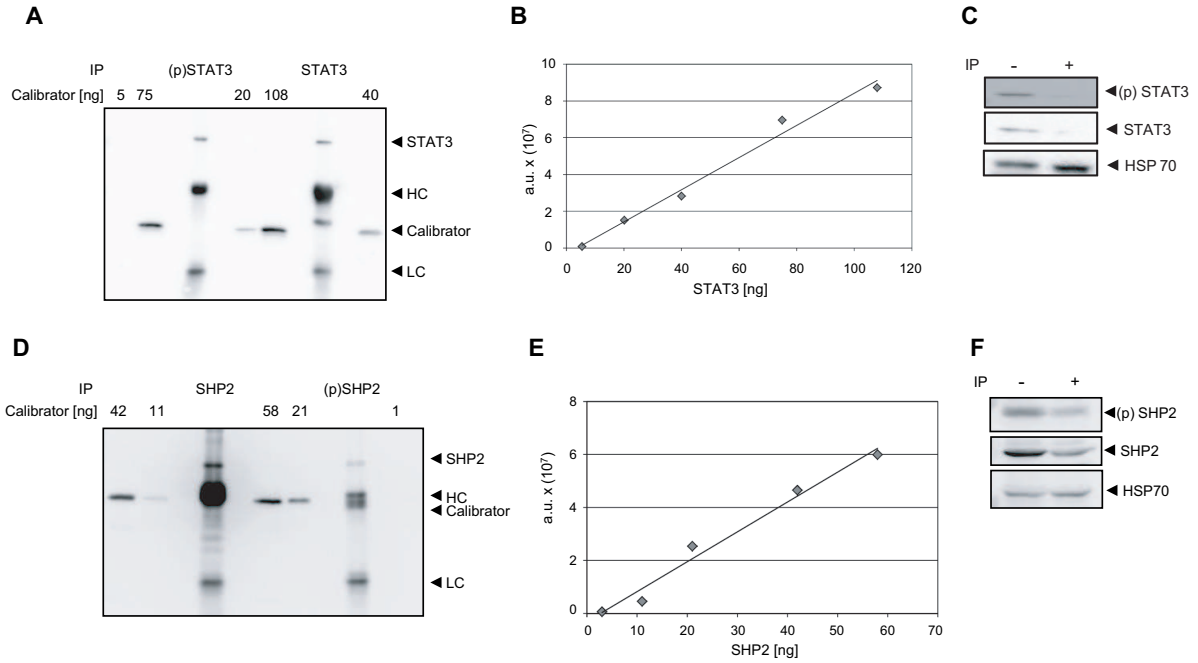


Figure S13: Quantification of SHP2, (p)SHP2, STAT3, and (p)STAT3.

The concentration of (p)STAT3, STAT3, (p)SHP2 and SHP2 was analyzed by quantitative immunoprecipitation using recombinant proteins as calibrators. Absolute amounts of (p)SHP2 and (p)STAT3 were calculated based on the precipitation of both species after stimulation with IL-6 (0,95 nM) for 6 minutes. Figure S13 A and D present representative immunoblots for STAT3 and SHP2, respectively. Representative standard curves for the calculation of absolute amounts of STAT3 and SHP2 are shown in Figure S13 B and E. Efficiency of immunoprecipitation was controlled in an aliquot of the lysate before and after immunoprecipitation Figure S13 C and F. Based on these analyses the concentration of STAT3 and SHP2 were calculated as 216 $\pm$ 62 nM and 222 $\pm$ 62 nM. The stimulation with IL-6 (6 minutes, 0,95 nM) resulted in 117 $\pm$ 32 nM (p)STAT3 and 67 $\pm$ 16 nM (p)SHP2. Mean $\pm$ SD are based on $n = 3 - 5$ independent experiments.

## Materials and Methods

### Quantification of intracellular species

For immunoprecipitation lysates were incubated with 1$\mu$g of antibody at 4°C over night (SHP2 (C18), STAT3 (C20), gp130 (M20)(Santa Cruz technologies, Santa Cruz, CA); pSTAT3-Y705, pSHP2-Y542 (New England Biolabs, Frankfurt am Main, Germany)). Subsequently, immunocomplexes were isolated using protein G dynabeads (Life technologies, Darmstadt, Germany) according to manufacturer‘s description. Efficiency of immunoprecipitation was controlled in an aliquot of the lysate before and after immunoprecipitation and taken into account for the calculation of the concentration. For quantification recombinant GST-tagged proteins containing the epitope of the corresponding detection antibody were used (GST-STAT3 (aa 670-770), abnova, Taipei, Taiwan), GST-SHP2-SH2 tandem domains (isolated from e. coli). We estimated the cell volume to be 500 fl based on the average cell diameter of trypsinized cells.

# Supplementary Information 7: Analysis of (p)STAT3 and (p)SHP2 in single cells.

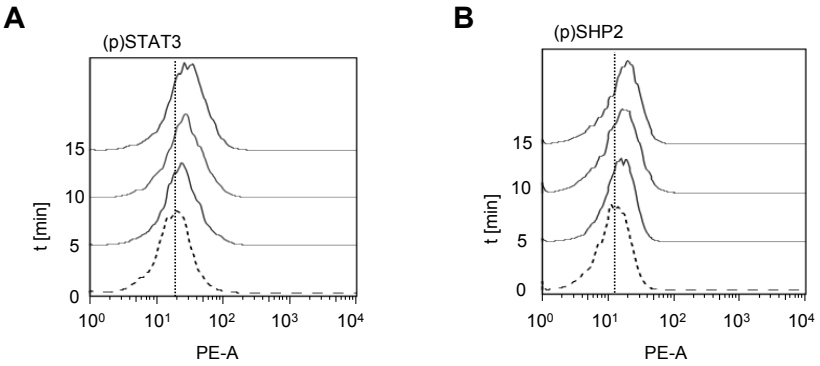


Figure S14: Analysis of (p)STAT3 (A) and (p)SHP2 (B) in single cells

To analyze if the cells react homogeneously to a stimulation with IL-6 the IL-6-induced phosphorylation of STAT3 and SHP2 was analyzed by intracellular FACS analysis. Phosphorylation of Jak1 could not be detected in intracellular FACS analysis (data not shown). HEK-gp80 cells were stimulated with a 6 minutes pulse of 0.95 nM IL-6 and fixed and permeabilised at the indicated time points. Phosphorylated STAT3 and SHP2 respectively were detected with specific antibodies against (p)STAT3 (A) and (p)SHP2 (B) and fluorescent secondary antibodies. In Figure S14 the fluorescence intensity is plotted at the x-axis,whereas the number of cells is plotted at the y-axis. To achieve a better comparability four time points (0,5,10,15 min) are plotted in one diagram. The background fluorescence of unstimulated cells is represented by dashed lines and vertical black lines. The phosphorylation of STAT3 and SHP2 rises within the first 5 minutes of stimulation and reaches a plateau at 10 minutes. The time courses of STAT3 and SHP2 phosphorylation are comparable between immunoblot (see Fig. 2 E and G) and intracellular FACS analysis shown here. In addition the FACS analysis shows that both STAT3 and SHP2 are homogeneously phosphorylated and that no subpopulations of cells with diverse phosphorylation patterns exist. Therefore, we conclude that the results obtained by immunoblotting do not represent an average of different subpopulations of cells but a good measure for the response of single cells.

# Materials and Methods

## Intracellular FACS Analysis

For intracellular FACS analysis cells were detached with PBS/EDTA (1:100) from cell culture dishes and immediately fixed with 2% paraformaldehyde (30 minutes, room temperature). Cells were washed twice in PBS containing 5% FCS and subsequently permeabilized with icecold 90% methanol (30 minutes). Cells were washed again and incubated with antibodies raised against (p)STAT3-Y705 and (p)STAT3-Y542 (New England Biolabs) (4°C). After 1h cells were washed again and subsequently stained with R-phycoerithrin-conjugated secondary antibody (Dianova, Hamburg, Germany) for 30 minutes. Cells were analyzed using the FACSCantoII (BD, Heidelberg, Germany). Data were analyzed using flowjo (Treestar, Ashland, OR, USA).

# Supplementary Information 8: Addition of second experiment for the first round of model refinement.

Note that no species in the Jak/STAT pathway is phosphorylated in the absence of IL-6 (see Figure 2 A, C, and F), such that the pathway is inactive. Therefore, we included an additional experiment, which consists of the following input/output specification:

$$u(t) = 0 \qquad t_1 = 15 \text{ min}$$

$$y_{2,1}(t_1) = \text{gp130}(t_0) \qquad y_{2,2}(t_1) = \text{SHP2}(t_0) \qquad y_{2,3}(t_1) = \text{STAT}(t_0)$$

$$y_{2,4}(t_1) = \text{pSHP2}(t_0) \qquad y_{2,5}(t_1) = \text{actGp130}(t_0) \qquad y_{2,6}(t_1) = \text{actSTAT}(t_0).$$

Note that $y$ is extended for an additional subscript, which allows to distinguish model outputs of different experiments. The measurements $\tilde{y}_{2,1} \dots \tilde{y}_{2,6}$, which correspond to the model outputs described in the equations above, represent the concentration of key species in the steady state – i.e. before stimulation. Since the steady state values of these key species have already been measured for determining the model's initial values, no additional measurements needed to be performed for this new experiment. Adding this experiment enforces that the six measured species remain in their initial steady state after 15 minutes. Parameter estimates, which violate the steady state will be penalized during parameter estimation.

# Supplementary Information 9: $M_0$ fails to describe data of IL-6 bound receptors.

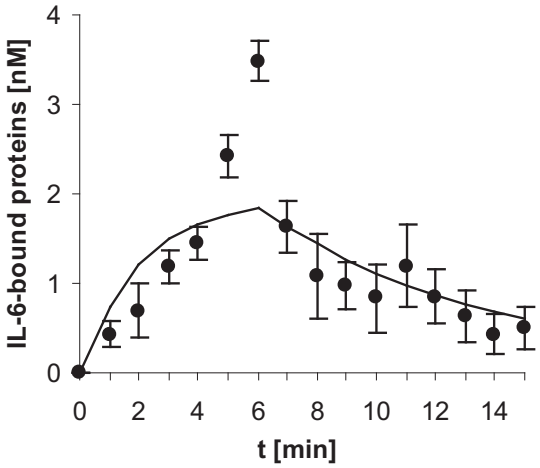


Figure S15: Discrepancy between the best fit of model $M_0$ to the data of IL-6-bound receptors. The best fit of $M_0$ resulted in a $\chi^2$ value of 84.6 with a $p$-value of 0.0022 and needed to be rejected. Model output $y_3$, which describes the IL-6-bound receptor species, is mostly responsible for the model/data mismatch. The graph shows the model output for $y_3$ (solid line) and the corresponding data points (black dots) over time.

# Supplementary Information 10: Optimal experimental design.

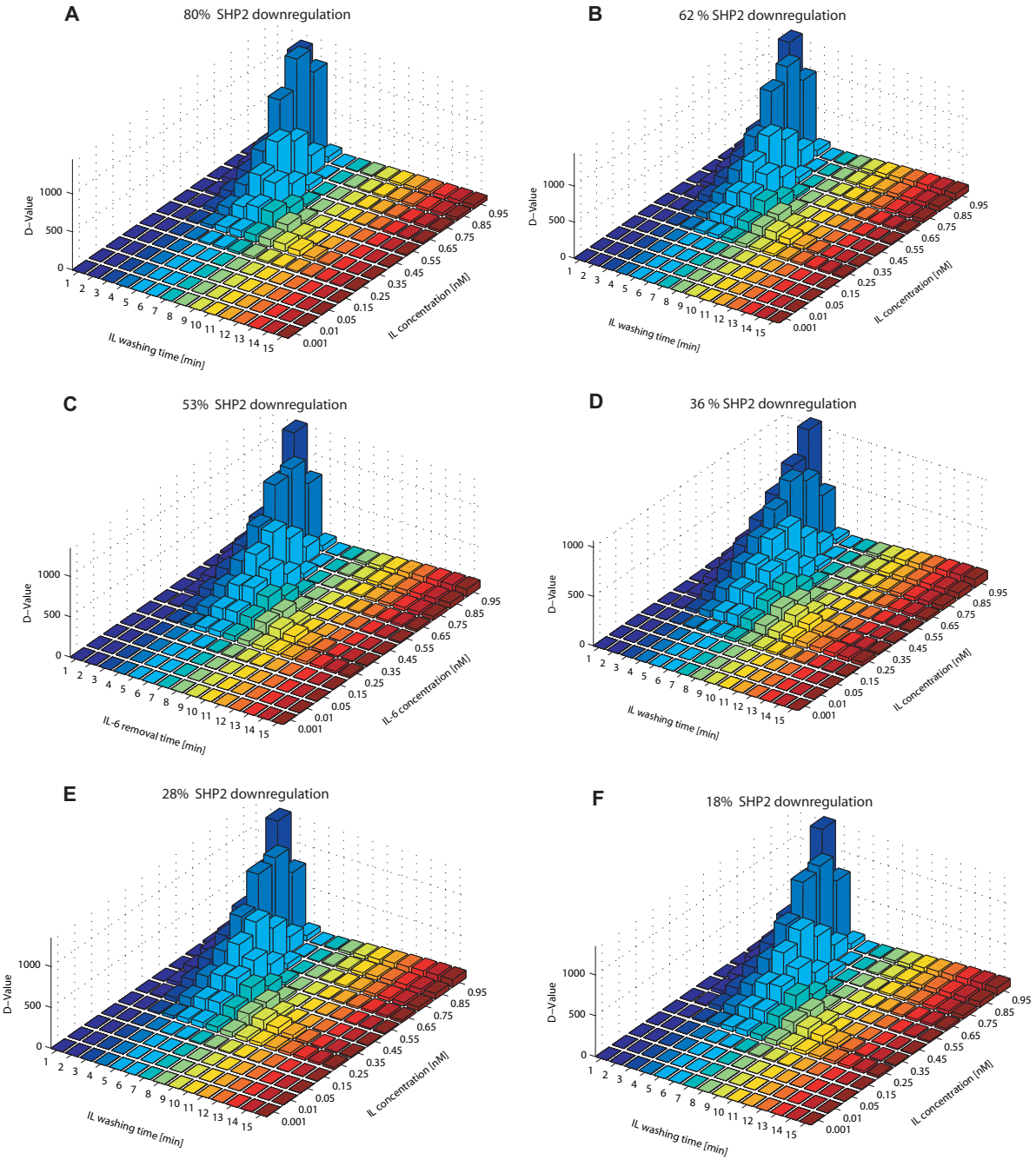


Figure S16: Results of optimal experimental design for different input pulses. In each graph, the $z$-axis shows the value of the D-optimality criterion, the $x$-axis specifies the time point for IL-6 removal and the $y$-axis defines the initial concentration of IL-6. The graphs (A to E) differ with respect to the downregulated SHP2 initial values.

# Supplementary Information 11: Approximation of the standard deviation of the second data set using the initial data set.

Whereas the initial data set consists of the mean value of repeatedly reproduced experiments ($n = 3 - 5$), the second data set consist of only one repetition, due to the limitations of the RNA interference technology. Consequently, the standard deviation of the second data set cannot be estimated from repeated measurements. Therefore, we use the largest average error of the initial data set ($\approx 40\%$) as the basis for an approximation of the standard deviation for the second data set. To reflect the fact that we have less confidence in the new experiment, compared to the well reproduced (n = 3-5) initial experiments, we doubled the largest average error for each output.

# Supplementary Information 12: Boundaries for actGp130_0.

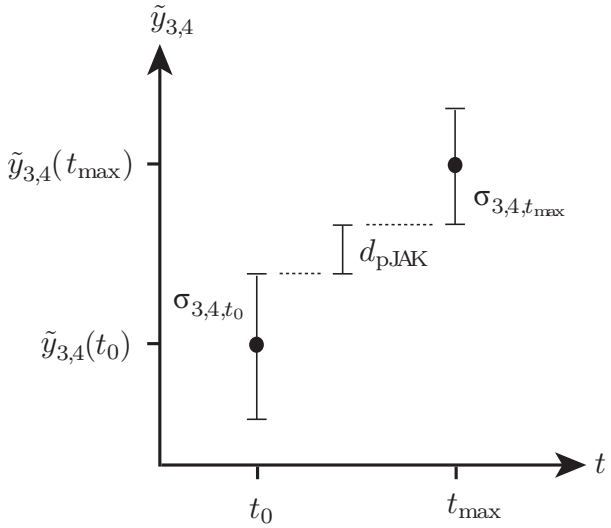


Figure S17: Visualization of $d_{\text{pJAK}}$. $d_{\text{pJAK}}$ represents a lower bound for the real difference between the initial ($\tilde{y}_{3,4}(t_0)$) and the maximal measurement ($\tilde{y}_{3,4}(t_{\max})$) of pJAK, because the minimal measurement is increased, while the maximal measurement value is decreased by the corresponding standard deviation $\sigma_{3,4,t_0}$ and $\sigma_{3,4,t_{\max}}$, respectively.

After fitting the model parameters to both the initial and the second data set, the resulting model predicts the pJAK concentration to be constant over time, thus not representing the increase of pJAK as shown by the data. This effect results from the fact that the estimated initial value for actGp130_0 reaches its upper bound i.e. the value of $\text{gp130}_{\text{Total}}$. Consequently, pJAK cannot further increase from its initial value, since all receptors are already activated. To be able to describe the increase of pJAK over time – as existent in the data – we established an upper estimation bound for actGp130_0 below $\text{gp130}_{\text{Total}}$. By this the pJAK concentration is forced to rise at least for the difference between this upper estimation bound and $\text{gp130}_{\text{Total}}$. We argue that a simulated time course of the pJAK concentration should be able to increase at least by a value equal to the difference between the initial measurement ($\tilde{y}_{3,4}(t_0)$) and the maximal measurement of pJAK ($\tilde{y}_{3,4}(t_{\max})$). We calculate this difference ($d_{\text{pJAK}}$) as

$$d_{\text{pJAK}} = (\tilde{y}_{3,4}(t_{\max}) - \sigma_{3,4,t_{\max}}) - (\tilde{y}_{3,4}(0) + \sigma_{3,4,t_0}) \text{ with } t_{\max} = \underset{t}{\operatorname{argmax}}\, \tilde{y}_{3,4}(t),$$

where $\sigma_{3,4,t_0}$ and $\sigma_{3,4,t_{\max}}$ denote the standard deviation of the $\tilde{y}_{3,4}(t_0)$ and $\tilde{y}_{3,4}(t_{\max})$, respectively. For a visualization of $d_{\text{pJAK}}$ see Figure S3. Note, that $d_{\text{pJAK}}$ can be interpreted as a lower bound for the real difference between the initial and the maximal measurement of pJAK, because the minimal measurement is increased, while the maximal measurement value is decreased by the corresponding standard deviation. By determining the ratio of $d_{\text{pJAK}}$ to the initial measurement of pJAK, we get a measure of how much increase from an initial value should be at least allowed. The resulting ratio for a minimal increase amounts to approximately $30\%$. Consequently, the upper estimation bound of actGp130_0 should amount to $70\%$ of $\text{gp130}_{\text{Total}}$ to allow the previously calculated minimal increase of $30\%$.

# Supplementary Information 13: $M_5$ is not able to adequately describe (p)SHP2 data.

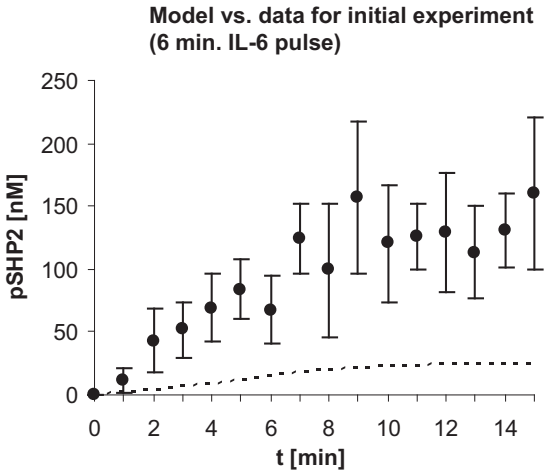


Figure S18: Model-data discrepancy for (p)SHP2 measurements from the first experiment. Measured values are represented by bold dots, while the model prediction of $M_5$ is represented by the dotted line. The model underestimates the SHP2 phosphorylation as given by the data in the first 15 minutes.

# Supplementary Information 14: $M_7$ with positive actR_IL feedback fails in providing biologically reasonable trajectories

Model $M_7$ with positive pSHP2 feedback replaced by positive actR_IL feedback – subsequently denoted as $M_8$ – results in a reasonable fit, but fails in providing biologically sound trajectories. We discuss the deficiencies of $M_8$ below.

$M_8$ predicts that in the second experiment significantly more actGp130 than actR_IL exists, even in the presence of IL-6. The amount of actGp130 remains above $73\%$, while the amount of actR_IL stays below $8\%$ of the total gp130 amount at all measurement times of the second experiment (see right graph in Figure part A of S19). Since it is known that IL-6 binding to the receptor is critical for pathway activation [2], the assumption that significantly more IL-6-free actGp130 exists during IL-6 stimulation than IL-6-bound actR_IL, is biologically not feasible. The reason for the abundance of actGp130 in the prediction of $M_8$ lies in the high values of the estimate of actGp130_0 ($73\%$ of the total amount of gp130). Despite this high initial value of actGp130, the measurement of pJAK, which reflects the amount of activated receptor, starts at a rather small value ($\approx 10\%$ of the total amount of gp130). Still, the model achieves an acceptable fit of the pJAK measurement, because the scaling factor for the pJAK measurement in the second experiment is 30 times smaller compared to the initial experiment (data not shown). Both measurements have been carried out on different WBs, such that different scaling factors are possible. However, as the same AB has been used, a 30-fold difference in measurement scaling is unlikely. Because of the high initial concentration of actGp130 and the small scaling factor of the pJAK measurement in the second experiment, the visually noticeable dynamics of receptor activation are not reflected by the model anymore (see Figure part B of S19). Model $M_8$ rather assumes a near constant level of active receptor, which is dominated by actGp130.

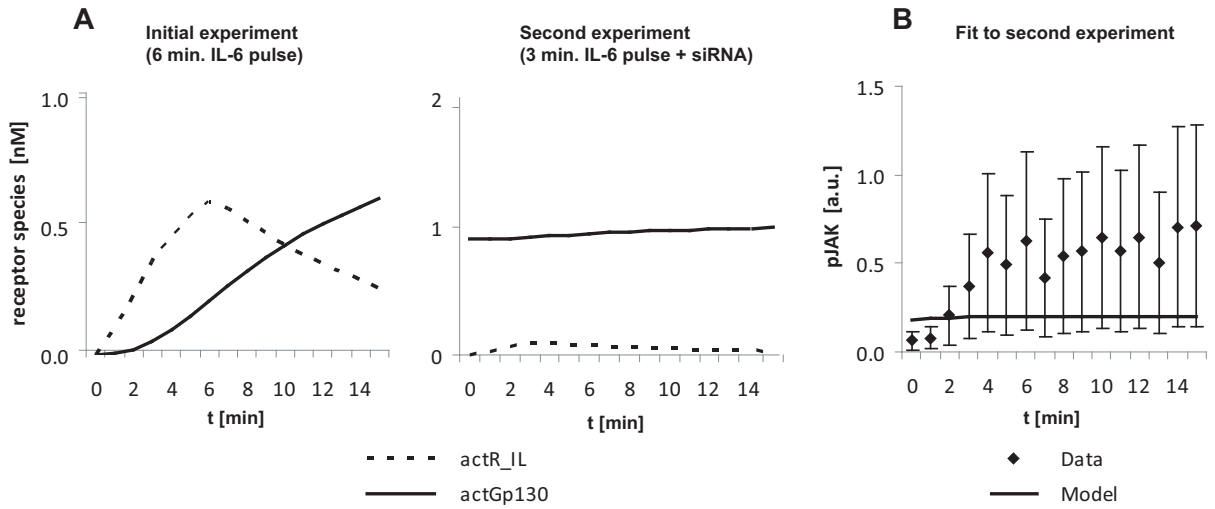


Figure S19: Properties of model $M_8$. The two graphs of part A depict the trajectories of actR_IL and actGp130 for the initial and the second experiment, respectively. The graph in part B of the figure shows the model fit to the pJAK measurement of the second experiment.

In summary, we reject $M_8$ for the following reasons:

1. Although IL-6 is the stimulating agent, the IL-6-induced pathway activation is only of minor importance in $M_8$.
2. The difference between the scaling factors of the pJAK measurement of the intial and the second experiment is too large in $M_8$.
3. The dynamic increase of the pJAK measurement in the second experiment is not represented sufficiently by $M_8$.

## References

[1] M. W. Pfaffl, *Nucleic Acids Res* **29**, e45 (2001).

[2] P. C. Heinrich, *et al.*, *Biochem J* **374**, 1 (2003).